Separating the pH-Dependent Behavior of Water in the Stern and Diffuse Layers with Varying Salt Concentration

Akemi M. Darlington, Tasha A. Jarisz, Emma L. DeWalt-Kerian, Sandra Roy, Sun Kim, Md. Shafiul Azam, Dennis K. Hore, and Julianne M. Gibbs

July 2017

Article

# Separating the pH-Dependent Behavior of Water in the Stern and Diffuse Layers with Varying Salt Concentration

Akemi M. Darlington, Tasha A Jarisz, Emma L Dewalt-Kerian, Sandra Roy, Sun Kim, Md. Shafiul Azam, Dennis Kumar Hore, and Julianne Montfort Gibbs

*J. Phys. Chem. C*, **Just Accepted Manuscript** • DOI: 10.1021/acs.jpcc.7b03522 • Publication Date (Web): 28 Jul 2017

# Separating the pH-Dependent Behavior of Water in the Stern and Diffuse Layers with Varying Salt Concentration

Akemi M. Darlington,[1] Tasha A. Jarisz,[2] Emma L. DeWalt-Kerian,[1] Sandra Roy,[2] Sun Kim,[1] Md. Shafiul Azam,[3] Dennis K. Hore,*[2] Julianne M. Gibbs *[1]

1. University of Alberta, Department of Chemistry, Edmonton, Canada 2. University of Victoria, Department of Chemistry, Victoria, Canada. 3. Bangladesh University of Engineering and Technology, Department of Chemistry, Dhaka, Bangladesh

**ABSTRACT:** Vibrational sum frequency generation (SFG) spectroscopy was utilized to distinguish different populations of water molecules within the electric double layer (EDL) at the silica/water interface. By systematically varying the electrolyte concentration, surface deprotonation, and SFG polarization combinations, we provide evidence of two regions of water molecules that have distinct pH-dependent behavior when the Stern layer is present (with onset between 10 and 100 mM NaCl). For example, water molecules near the surface in the Stern layer can be probed by the *pss* polarization combination, while other polarization combinations (*ssp* and *ppp*) probe predominantly water molecules further from the surface in the diffuse part of the electrical double layer. For the water molecules adjacent to the surface within the Stern layer, upon increasing the pH from the point-of-zero charge of silica (~pH 2) to higher values (~pH 12) we observe an increase in alignment consistent with a more negative surface with increasing pH. In contrast, waters further from the surface appear to exhibit a net flip in orientation upon increasing the pH over the same range, which we attribute to the presence of the Stern layer and possible overcharging of the EDL at lower pH. The opposing pH-dependent behavior of water in these two regions sheds new light on our understanding of the water structure within the EDL at high salt concentrations when the Stern layer is present.

## INTRODUCTION

A foundational concept in colloid and surface chemistry has been that of the electric double layer (EDL), which describes how charged surfaces impact the composition of the adjacent liquid layer as well as the local concentration of electrolyte ions that counter the surface charge. In 1913, Gouy and Chapman proposed that this EDL consisted of a charged surface and a diffuse layer of counterions enriched near the surface with an excess in concentration that decayed exponentially away from the surface until equaling the bulk concentration of ions.[1] Later Stern and Grahame argued that at high enough salt concentrations, a dynamic layer of counter ions would form at the surface that could act as a parallel plate capacitor such that the potential decayed linearly between the surface and this wall of counterions,[2-4] often referred to as the compact part of the EDL, or the Stern layer.[2] Thereafter the diffuse layer, similar to that proposed by Gouy and Chapman, neutralizes all remaining charges. This Gouy-Chapman-Stern-Grahame EDL model has been widely utilized since its inception and provides a rationale for the difference in the high surface potentials of mineral oxides based on the surface charge densities measured by potentiometric methods[5-6] and the lower in magnitude zeta potentials, measured outside the Stern layer by electrokinetic techniques.[7-8]

Only recently, however, have techniques emerged that are able to quantitatively disentangle the potential at different layers of the EDL in colloid systems. For example, Brown and co-workers utilized x-ray photoelectron spectroscopy (XPS) to measure the potential at the silica surface and compare it with zeta potential measurements from electrokinetic methods using a microjet technique that allows colloids to be directly probed by XPS. From a comparison of the surface potential and the zeta potential, the authors were able to determine the thickness of the Stern layer as a function of ion identity[9-10] and salt concentration.[11] The authors found that by 100 mM NaCl, the Stern layer consisted of less than one water molecule between the silica surface and the hydrated sodium at pH 10 and this salt concentration.[11]

These potential measurements have provided compelling evidence of the existence of an average interfacial structure in line with the model first derived by Stern and Grahame of a compact layer as well as a diffuse layer. Yet, in these studies the molecular structure of the EDL is not directly measured but only inferred from the potential measurements. To directly probe the molecular structure, surface-specific infrared measurements, such as vibrational sum frequency generation (SFG), would be well-suited to probe water molecules in both the diffuse and compact parts of the EDL. SFG has been widely utilized to monitor the hydrogen-bonded structure and extent of ordering of interfacial water at a variety of interfaces ranging from amphiphilic films suspended at the air/aqueous interface[12-15] to mineral oxides like silica[16-24] and alumina.[25-27] Moreover, SFG has also shown that the presence of salt perturbs the interfacial water structure, with increasing salt concentration leading to a decrease in the amount of ordered water.[18-20, 22-23] This phenomenon can be attributed to increased screening of the surface potential, thereby decreasing the electrostatic force aligning the water dipoles, which is consistent with EDL models.[19]

Only recently, however, has SFG been utilized to study different interfaces in terms of the Stern layer, or the water layer directly adjacent to the surface.[28-30] At the silica/water inter-

face, Lovering et. al. showed that the structure of water in the Stern layer is dependent on the ion identity. The authors found that the Stern layer could be completely disrupted at high divalent salt concentrations at neutral pH based on the absence of SFG water intensity, yet the same ionic strength of monovalent salts did not show this effect.[30] This led to the development of an ion-identity dependent EDL model to rationalize the behavior of these salts at high concentrations. In another recent study that was performed at lower salt concentrations, the influence of pH on both the diffuse and surface water layers was probed with SFG at a charged monolayer film suspended at the air/water interface.[28] Using EDL models to determine the static electric field at the monolayer surface, the authors developed a method to subtract the contribution of the diffuse layer from the water spectra to isolate the Stern layer structure, which they referred to as the bonded interfacial layer.[28] Although changes at low pH (~pH 2) and high pH (> pH 10) were observed in the bonded interfacial layer in the absence of added electrolyte, the influence of salt concentration on this surface layer was not discussed.

These SFG experiments at the air/ charged monolayer/water interface modeled the pH-dependent behavior by including a phase shift term between the signal originating from the surface-adjacent water and those further from the surface in the diffuse layer.[28, 31-32] In related second harmonic generation (SHG) experiments performed off resonance at the oil/aqueous interface, Gonella et. al. found that the interference between the same two terms described by this phase shift was significant at lower ionic strengths (< 1 mM) owing to the large volume probed when the Debye length is long and the diffuse layer extends deep into the bulk (~>10 nm).[31] However, this interference between the surface and the "bulk" became negligible at higher ionic strengths owing to the reduced Debye length.[31] Relatedly, phase-sensitive SHG measurements at low salt concentration confirmed that much of the signal originated far from the surface at the α-quartz/water interface in the presence of a constant low salt concentration of 3 mM. The authors confirmed an imaginary component to the SHG response that interfered with the reference signal from bulk quartz, which they attributed to bulk water far from the surface.[32] However, working at higher salt concentrations should limit such interference between the surface and the diffuse layer as the Debye length becomes less than 1 nm [NaCl] ≥ 10 mM. At such higher salt concentrations any interference between the surface water and the diffuse layer should instead originate from the overall assembly of the interface and not from a phase-factor based on the distance probed from the surface.

Here we perform pH-variation experiments at multiple salt concentrations to understand the interplay between the surface charge density and high salt concentration on the structure of the EDL. In several of our experiments, a constant high salt concentration is maintained to ensure that the compact part of the EDL is present throughout our experiments. As will be shown, the pH-dependent trends of two different water vibrational modes vary substantially at higher salt concentration, which has never before been reported. This combination of high salt concentration and pH variation supports previous studies that suggest that there are different water populations within the different layers of the EDL.[11, 18] Moreover, the results shown here provide the first molecular evidence that waters within the different layers of the EDL experience different orienting forces. Finally, the high salt concentrations used avoid any complex phase relations described above between the surface and bulk response providing a clearer picture of the pH dependence of the water immediately at the surface and that nearby in the diffuse layer.

## RESULTS AND DISCUSSION

### Vibrational SFG Theory.

In vibrational SFG, light from a mid-IR source and light from a visible or near-IR source are combined at an interface and generate light that is the sum of the two incident light sources. When the frequency of the IR light closely matches the vibrational resonance of a molecule at an interface, the resulting SFG response can be greatly enhanced.[33] Moreover, the polarization of the incident light fields determines the SFG response, which is related to the orientation of molecules at the interface and the symmetry of the resonant vibration. For example *ssp* polarization refers to *s*-polarized SFG, *s*-polarized visible and *p*-polarized IR, where *s*-polarized and *p*-polarized describe linearly polarized light with the electric field oscillating perpendicular or parallel to the plane of incidence, respectively.[34] As shown in Figure 1, the *s*- and *p*- directions of the incident or sum frequency electric fields can be related to the Cartesian coordinates of the lab frame and consequently the overall orientation of molecules assembled at the interface.

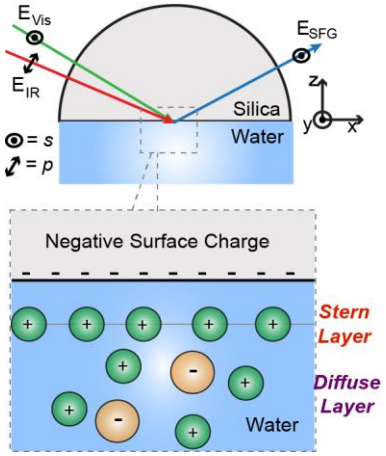


**Figure 1.** Depiction of SFG generated at the interface between silica and water. In the diagram the *ssp* polarization combination (*s*-polarized SFG, *s*-polarized visible, and *p*-polarized IR) is shown. *S*-polarized and *p*-polarized refer to light with its electric field component oscillating perpendicular to the plane of incidence (in and out of the page, double circle) or parallel to the plane of incidence (double headed arrow). Inset: a close up of the different layers of the electric double layer (EDL). The layer of ions and water nearest to the surface make up the Stern layer; beyond that is a diffuse layer of ions that neutralize any remaining charge such that the EDL is electroneutral.

The SFG intensity ($I_{SFG}$) is determined by the incident electric fields ($E_{Vis}$ and $E_{IR}$) from the laser source and the second-order susceptibility ($\chi^{(2)}$), related to the composition and net orientation of molecules assembled at the interface. The parameter $\chi^{(2)}$ is made up of 27 tensor elements based on combinations of the Cartesian coordinates x, y, and z.[35] Moreover, because of the symmetry of the silica/water interface, only 7 of the 27 tensor element are non-zero. One of these non-zero tensor elements for the silica/water interface is $\chi^{(2)}_{yyz}$ (probed by $\chi^{(2)}_{ssp}$), which describes the efficiency of generating SFG with the electric field polarized in the y direction with incident y-polarized visible and z-polarized IR. Accordingly, the average orientation of molecules as well as the symmetry of the vibrational mode in resonance determines which of the non-zero $\chi^{(2)}$ tensor elements is large.

$$I_{SFG} \propto \left|\chi^{(2)} E_{Vis} E_{IR}\right|^2$$

$$\chi^{(2)} = \chi^{(2)}_{NR} + \chi^{(2)}_{R} = \chi^{(2)}_{NR} + \sum \frac{A}{\omega_0 - \omega_{IR} - i\Gamma}$$

Under the electric dipole approximation, $\chi^{(2)}$ is non-zero only when there is a break in inversion symmetry, which accounts for the intrinsic surface selectivity of this technique. For vibrational SFG, $\chi^{(2)}$ is made up of a non-resonant and resonant component, $\chi_{NR}{}^{(2)}$ and $\chi_{R}{}^{(2)}$. The latter can be described by the sum of Lorentzian functions, where *A* is the amplitude (which is proportional to the number of molecules in resonance as well as their average orientation), $\omega_{IR}$ is the incident IR frequency, $\omega_0$ is the resonant frequency of the vibrational mode and $\Gamma$ is the homogeneous line width. The dependence of *A* on the average orientation means that only water with a net orientation resulting from interactions with the surface will give rise to SFG signal, while no signal will arise from the bulk, isotropic water.

The silica/water interface adds another level of complexity to these equations because of silica's ability to become charged via deprotonation or protonation of surface silanols.[36] Above pH 2, the surface of silica has a net negative charge, which results in a static electric field and an interfacial potential ($\Phi_0$) that can also generate SFG via the third order susceptibility ($\chi^{(3)}$).

$$I_{SFG} \propto \left|\chi^{(2)} E_{Vis} E_{IR} + \chi^{(3)} E_{Vis} E_{IR} \Phi_0\right|^2$$

The $\chi^{(3)}\Phi$ term results from water molecules that are aligned or polarized as a result of interaction with the interfacial potential.[19, 22, 37-38] The magnitude of the interfacial potential felt by the water molecules can be modulated by changing the pH of the bulk solution, which changes the degree of protonation of the silica, or by changing the concentration of electrolyte, which changes the amount of screening of the negative surface charges. As such, by employing high salt concentrations, we can utilize SFG to study the interplay of surface deprotonation and electrolyte screening on the structure of water within the EDL created at the interface.

**pH-Variation Experiments with 0.1 M NaCl.**

Below 100 mM concentration for monovalent ions, the Gouy-Chapman model of the EDL is often utilized, which neglects the compact part of the EDL and considers only the diffuse layer.[39] Above 100 mM, however, the compact part of the EDL must be considered to properly model the interface. Thus, we first explored the effects of 100 mM NaCl salt concentration on the water structure at the silica/water interface as we varied the bulk pH using the *ssp* polarization combination (Figure 1A). The water *ssp*-SFG spectra at the silica interface near neutral pH generally contain two distinct peaks in the OH stretching region: one at 3200 $cm^{-1}$, the other at 3400 $cm^{-1}$ (Figure 2A). Previous pH variation studies of the silica interface performed by Ostroverkhov, Waychunas and Shen observed an increase in *ssp*-SFG intensity upon increasing the pH from pH 2.0 to 12.0 at the silica interface in the presence of low electrolyte concentrations.[17] These results were consistent with reports of a point of zero charge (pzc) of silica between pH 2-3,[36] as there should be no surface potential at the pzc, and therefore no electrostatic force aligning water molecules at the interface leading to a minimum in the SFG. Yet above the pzc the silica surface is deprotonated, and increasing the pH increases the magnitude of the surface potential and consequently the amount of aligned water. However, when we performed similar measurements at higher electrolyte concentration (100 mM NaCl), a non-monotonic change in *ssp*-SFG intensity with varying pH was observed with a minimum in the intensity at ~pH 5 instead of pH 2 (Figure 2A). As the only significant difference in our two experiments was the electrolyte concentration, we attributed the non-monotonic behavior in this pH-variation experiment to the presence of the higher concentration of NaCl.

There is some precedent for observing non-monotonic changes in SFG intensity with increasing pH. SFG experiments on alumina showed that at the point of zero charge a minimum in the *ppp*-SFG intensity was observed with varying pH.[25-26] At pH values below this minimum, the authors proposed the water had opposite orientation to that at higher pH owing to the change in sign of the alumina surface (positive below the pzc and negative above the pzc).[26] Consequently, one possibility is that most of the water molecules contributing to the *ssp*-SFG spectra are flipping orientation upon going from pH 2 to pH 12 in the presence of 0.1 M NaCl.

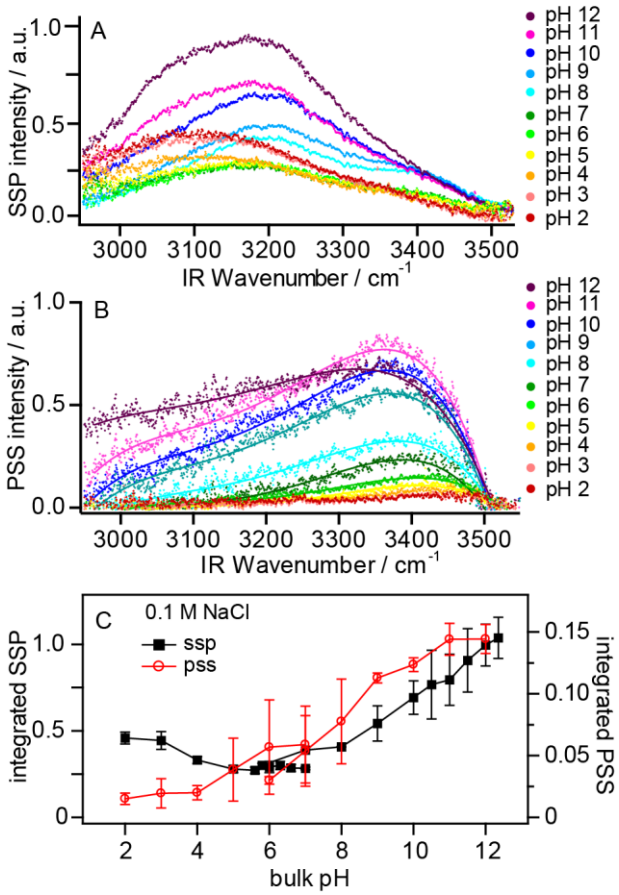


**Figure 2.** Broadband (fs) SFG intensity as a function of pH at the silica/aqueous interface with 100 mM NaCl. A) Representative pH titrations using the *ssp* polarization combination. B) Representative pH titrations using the *pss* polarization combination. C) Integrated SFG intensity versus pH for the two different polarization combinations. The spectra were integrated from 2950-3550 $cm^{-1}$, and the average values and standard deviation from at least two replicates are reported.

To determine if this unexpected pH-dependent behavior was influenced by the sensitivity of *ssp*-SFG to the average orientation (i.e. twist and tilt angle) of the oriented water, we also performed experiments with the *pss* polarization combination (Figure 2B), which probes a different $\chi^{(2)}$ tensor element. For the *pss* polarization combination the SFG signal intensity of the water molecules generally increased from pH 2 to 12 (Figure 2C). This was in marked contrast to the pH dependence of the *ssp*-SFG where we observed a factor of four increase in

integrated intensity upon increasing the pH from ~pH 6 to pH 12 and, most notably, a factor of two increase upon *decreasing* the pH from neutral pH to pH 2 (Figure 2C). Not only was the trend in the SFG response different for the *ssp* and *pss* polarization combinations, but the shape of the SFG spectra were also very different. Specifically, the *ssp*-polarized SFG spectra were dominated by the 3200 $cm^{-1}$ peak, while the *pss*-polarized SFG spectra were dominated by the 3400 $cm^{-1}$ peak (Figure 2A and 2B, respectively). This effective absence of the low wavenumber mode in the *pss*-SFG of $D_2O$ and the *sps*-SFG of $H_2O$ (equivalent to *pss*-SFG) has been observed in previous reports.[18, 40-41] In addition, the *ssp*-SFG spectra at the lower pH values appear to red shift compared to the *ssp*-SFG spectra at higher pH.

**Effect of Different NaCl Concentrations.**

If salt is the cause of the unusual pH trend observed in the *ssp*-SFG response of water molecules then we reasoned that increasing the salt concentration might further affect the SFG. IR-scanning (ps) SFG measurements at 500 mM NaCl are shown in Figure 3A over a broader range of incident IR that reveal a significant contribution in intensity at even lower IR wavenumber (<3000 $cm^{-1}$), which increases with decreasing pH (Figure 3A) consistent with our observations at 100 mM. In addition, there also appears to be a small contribution around 3600 $cm^{-1}$ at all pH values studied, which is thought to arise from silanol that is weakly hydrogen-bonded but still exchangeable with other water.[24, 41] Overall, the pH-sensitivity of the *ssp*-SFG was similar to that observed at lower salt concentration; the SFG intensity decreased from pH 2 to 7, where it reached a minimum in intensity. Increasing the pH further, resulted in an increase in the SFG intensity revealing non-monotonic behavior with changing pH. Similar non-monotonic behavior was observed in broadband SFG experiments from 500 mM NaCl shown in Figure 3B.

At both of these higher salt concentrations (100 mM and 500 mM NaCl), we expect the formation of a Stern layer, with less of a contribution from the diffuse layer as the Debye length decreases with increasing salt concentration. At 10 mM, however, the EDL is typically described by the Gouy-Chapman model, which neglects the compact part of the double layer as the diffuse layer should dominate as a result of the longer Debye length.[1, 39] Therefore, we performed the same pH titrations with 10 mM NaCl to compare how the *ssp*-SFG varied in both the high salt and low salt regimes. This experiment was most similar to what Osteroverkhov et al. had previously examined for the pH-dependent SFG at the silica/water interface.[17]

Figure 3B illustrates the average integrated intensity of the *ssp* polarized SFG as a function of salt concentration. For the interface at low salt concentration (10 mM), the average integrated SFG intensities between pH 2.0 to 4.0 were all within one standard deviation of each other consistent with the previous report at this salt concentration where the minimum was observed between pH 2 and 3.[17] In contrast, the *ssp*-SFG minimum shifted to pH 5 and then to pH 7 with 100 mM and 500 mM NaCl, respectively, providing further support that this unusual behavior stemmed from the presence of salt. Furthermore, at higher pH (pH > 8) we also observed that the *ssp*-SFG signal intensities increased with decreasing salt concentration. This overall trend in salt concentration and SFG intensity at higher pH is consistent with greater screening of the negative surface charges at the higher salt concentrations by the $Na^+$, as expected from previous salt variation SFG studies.[18-19, 23] The trend at lower pH, however, cannot be rationalized by simple screening arguments as the 100 and 500 mM NaCl both had significantly more signal intensity than the interface with 10 mM NaCl.

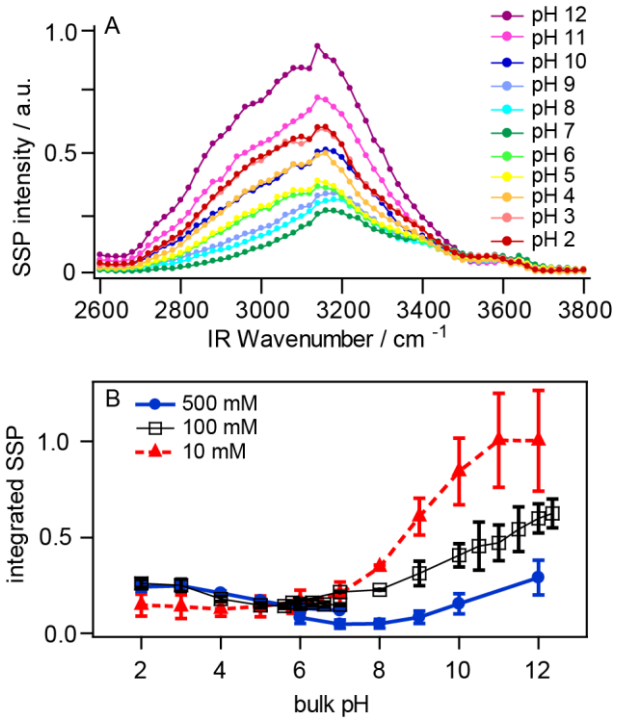


**Figure 3**. A) A representative scanning (ps) *ssp*-SFG titration of the silica/aqueous interface with 500 mM NaCl. B) Average integrated broadband (fs) *ssp*-SFG intensity as a function of pH with NaCl concentrations of: 500 mM (blue circles), 100 mM (black squares), and 10 mM (red triangles). The error bars are the standard deviation from two or more experiments.

We next explored the other polarization combinations at 500 mM NaCl to understand how the water molecules in each polarization combination responded to the change in pH in the presence of this high salt concentration (Figure 4). Interestingly, the trend in *ppp*-SFG intensity with pH was very similar to that observed for *ssp*, possibly indicating that the same tensor element contributed the most to both polarization combinations (Figure 4A and C). Once again, the *pss*-SFG exhibited minimum intensity at low pH consistent with the 100 mM *pss*-SFG data (Figure 4B and 2B, respectively).

In all of our *ssp*-SFG measurements, we observed that the mode at 3200 $cm^{-1}$ dominated the spectra, while *pss*-SFG exhibited a clear peak at 3400 $cm^{-1}$ with the observed increase in intensity at low wavenumber most consistent with an increase in non-resonant SFG (Figure 2B). Although it is generally considered that each peak is associated with populations of water in different hydrogen-bonding environments, in the literature there has been debate over their exact origin. The two peaks were first thought to be two different hydrogen bonding structures of the water molecules, where the 3200 $cm^{-1}$ and the 3400 $cm^{-1}$ were described in terms of "ice-like" (strongly h-bonded) and "liquid-like" (weakly h-bonded) environments, respectively.[16] Subsequently, researchers suggested that the 3200 $cm^{-1}$ could be the symmetric stretch and the 3400 $cm^{-1}$ could be the asymmetric stretch of water, meaning that both modes could stem from the same water population.[42-44] Further studies at the silica/HOD interface revealed differences with the silica/$H_2O$ interface that also caused the authors to suggest that the 3200 $cm^{-1}$ and 3400 $cm^{-1}$ modes were coupled

and therefore originating from the same water populations; specifically, they assigned them to a Fermi resonance between the symmetric stretch of water and the overtone of a water bend.[40] A more recent study, however, supported the original argument that the 3200 $cm^{-1}$ and 3400 $cm^{-1}$ have contributions from two different populations of water molecules at the silica surface as the salt dependence of each peak was found to be different, which is difficult to rationalize for coupled modes.[18] Furthermore, phase sensitive measurements of the silica/HOD interface reveal two vibrational OH stretching modes, which cannot be coupled owing to the different symmetry of HOD vs $H_2O$ suggesting that these two modes represent different hydrogen-bonding environments of the HOD.[45] Additional evidence that the 3400 $cm^{-1}$ peak is at least partly associated with a separate water species is provided by experiments performed at the air/water interface.[44] SFG of this interfacial water in *sps* polarization combinations revealed no SFG intensity near 3400 $cm^{-1}$,[44] the complete absence of which is not likely if the 3400 $cm^{-1}$ intensity stems from an asymmetric mode of water as such a mode's symmetry would lead to large intensity for the *pss* and *sps* polarization combinations at most tilt angles.

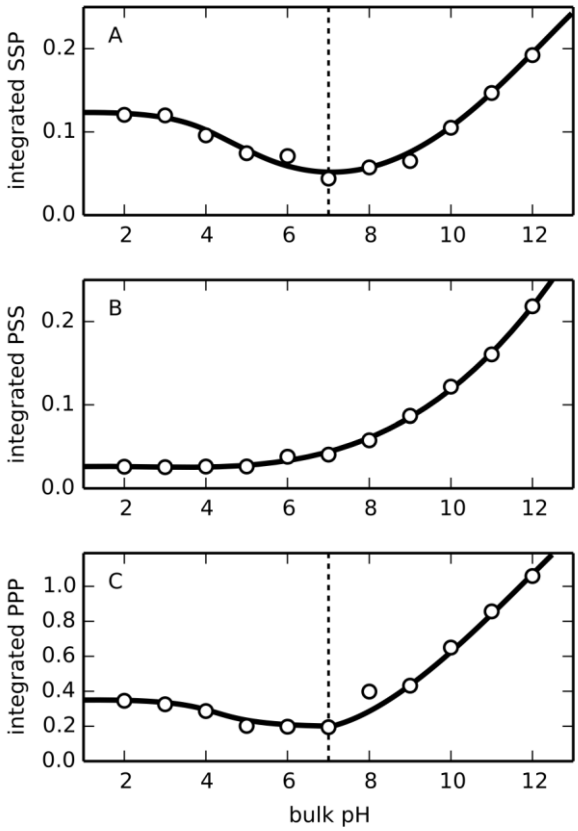


**Figure 4.** Integrated SFG intensity of all 500 mM titrations using A) *ssp*, B) *pss* and C) *ppp* polarization combinations.

**Model 1: Change in Orientation of Water with Varying pH.**

We reasoned that the dominance of the 3200 $cm^{-1}$ peak in the *ssp* and *ppp* spectra and the 3400 $cm^{-1}$ peak in the *pss* spectra were due to the average orientation of water associated with each vibrational mode. Moreover, as the trends with increasing pH are markedly different for the two bands, it is possible that these two water populations are also changing orientation differently in the two environments as the pH is changed. MD simulations provide support for a change in pH leading to a change in orientation as both the tilt and twist angles of water, as well as the width of the angular distributions, were observed to vary with surface hydrophobicity and charge.[46-47] Therefore, to test whether systematic changes in tilt angle could account for the pH-dependent behavior, we simulated SFG spectral intensity as a function of the water molecule orientation. (A depiction of the twist and tilt angles of water molecules at a surface are shown in Figure 5.) This simulation requires knowledge of the vibrational hyperpolarizability, $\alpha^{(2)}$. Since we are dealing with condensed phase water, such information is not as readily accessible due to the intramolecular coupling being sensitive to the hydrogen bonding environment at the surface. As mentioned, the spectral intensity at 3200 $cm^{-1}$ and 3400 $cm^{-1}$ has contributions from many types of OH oscillators, including modes that are coupled and those that are uncoupled. We have addressed this by performing molecular dynamics simulations of water next to a model hydrophilic interface which allows us to capture all of the different species as well as coupled modes contributing to these two spectral regions. Further details of this procedure are provided in the experimental section. As shown in Figure 6A and 6B, the *ssp* and *pss* intensity as a function of the water tilt and twist angles for the 3200 $cm^{-1}$ mode are nearly anti-correlated, such that orientations that yield significant *ssp* signal at 3200 $cm^{-1}$ lead to no *pss* signal. Hence it is likely that the waters corresponding to the 3200 $cm^{-1}$ mode are oriented such that they are not probed by the *pss* polarization combination. In contrast, the *ssp* and *pss* intensity maps of the 3400 $cm^{-1}$ mode are not mutually exclusive, so there are multiple orientations that lead to signal intensity in both polarization combinations. This was consistent with the appearance of the 3400 $cm^{-1}$ mode in both *ssp* and *pss* spectra although the former was dominated by the 3200 $cm^{-1}$ mode.

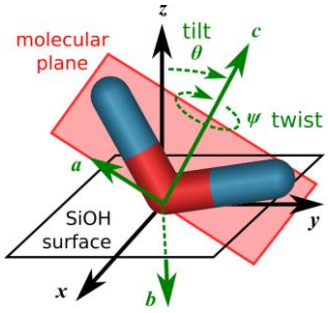


**Figure 5.** Illustration of the water molecule orientation with respect to the (x,y) plane of the surface, where z is the outward-facing surface normal, pointing into the bulk water solution. The tilt angle theta is defined with respect to the H-O-H bisector, the molecular symmetry axis, c. Theta (θ) is the angle between c and z. The twist angle psi (ψ) represents the rotation about c.

As mentioned, the minimum in SFG intensity is suggestive of a flip in the water molecule orientation as a function of pH, which in this reorientation model would involve a tilt angle change that passes through θ=90°. Therefore we asked, within the constraints of this model, could the *same* change in orientation for the two different populations explain the pH-dependent trends for the different polarization combinations? If the differences observed cannot be attributed to the same change in twist and tilt angles, it provides evidence that the two modes (3200 $cm^{-1}$ and 3400 $cm^{-1}$) are experiencing different orienting forces such that each water population is being ordered to a different extent or oriented in a different direction. From the simulations we see that for water molecules in

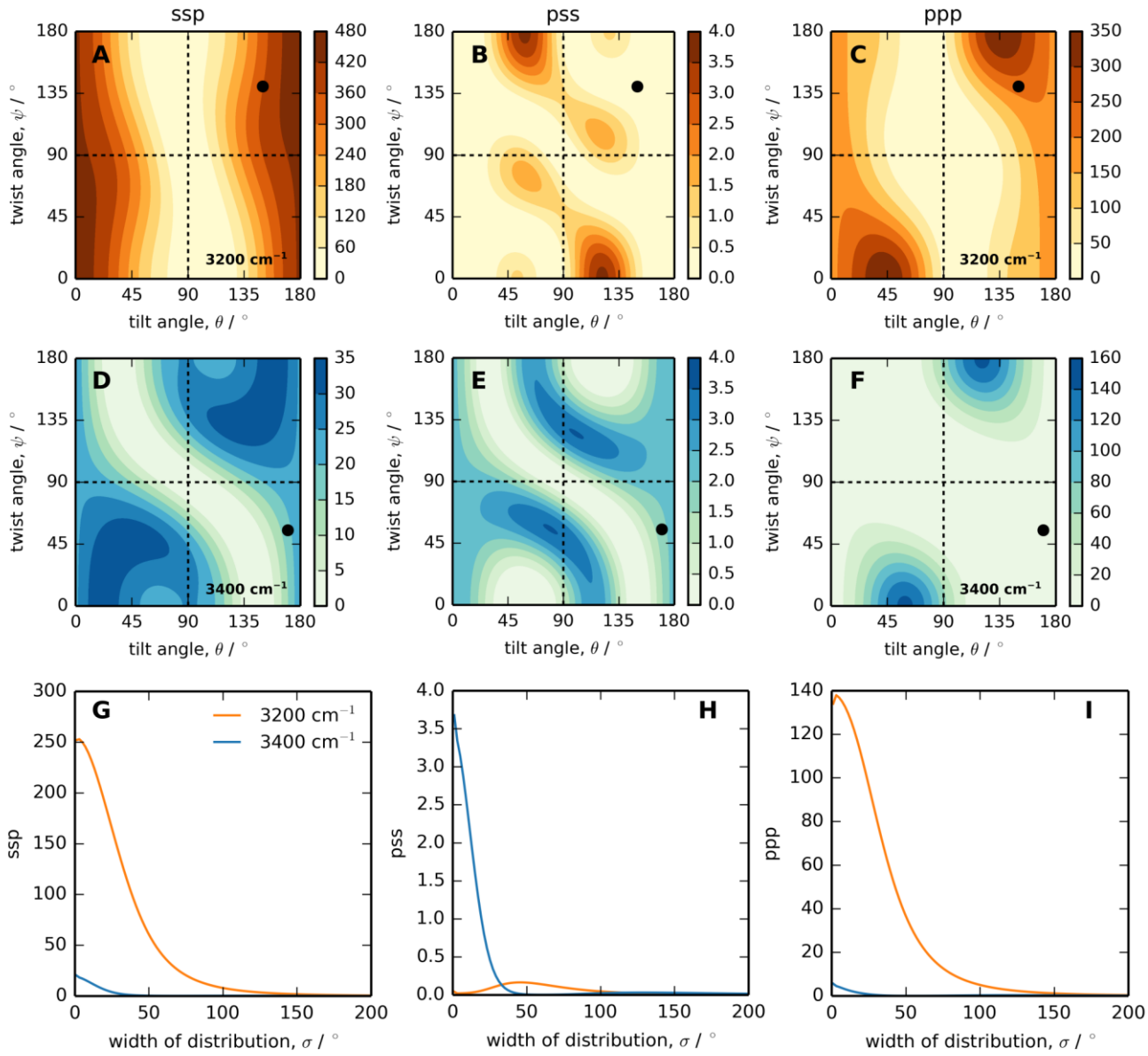


**Figure 6.** Predicted SFG intensity for water next to an OH-terminated surface in the (A) ssp, (B) pss, and (C) ppp polarizations for the mode at 3200 $cm^{-1}$, as a function of the molecules tilt and twist angles (as illustrated in Fig. 5), assuming a narrow distribution about these angles. For a 3400 $cm^{-1}$ water species, the results for these same polarizations are shown in Figure 6D-F. Considering a (θ=150°, ψ=140°) orientation for the 3200 $cm^{-1}$ species (as indicated by the black dot in the top row, which corresponds to θ, ψ at pH 12) and a (θ=170°, ψ=55°) orientation for the 3400 $cm^{-1}$ species (black dot in the middle row), we can predict the variation in SFG intensity as the width of the tilt and twist angle distributions (assumed to be the same) increases. This is shown in the bottom row (G-I).

the 3200 $cm^{-1}$ region, the *ssp* and *ppp* polarized spectra show similar trends for a given set of orientations (Figure 6A and 6C). Moreover, for twist angles between 90–140° and an initial tilt angle of ~ 40°, there is a continual decrease in spectral intensity for *ssp*- and *ppp*-SFG with increasing tilt angle until a minimum is reached, followed by an even greater increase in intensity. This non-monotonic change in spectral intensity as a function of tilt angle is consistent with the *ssp* and *ppp* experimental spectra at high salt concentrations, which also show a decrease then increase in spectral intensity with increasing pH. Accordingly, the trend in the *ssp* and *ppp* experimental spectra could be explained by a small initial tilt angle of these water molecules, which then increases systematically with pH such that a flip in orientation is observed (i.e. the tilt angle increases beyond 90°). Since the *pss* spectra are not sensitive to the 3200 $cm^{-1}$ mode, the relatively constant intensity observed at these twist angles is also consistent with the data (Figure 6B).

For the 3400 $cm^{-1}$ mode, the *pss* polarization scheme is the most sensitive probe as it nearly excludes the 3200 $cm^{-1}$ water population. Thus we examined our water orientation model to determine if the same changes in orientation of the 3400 $cm^{-1}$ water are consistent with increasing SFG intensity with increasing pH. However, there are no twist angles that lead to a systematic increase in intensity upon changing the tilt angle through 90°, consistent with a flip in orientation. Instead, for the mode at 3400 $cm^{-1}$, assuming a twist angle between 45° and 55°, a systematic increase in the tilt angle from ~140° towards 180° would result in an increase in intensity with increasing pH. These tilt and twist angle combinations were chosen based on similar (within 10°) values reported in previous experimental data at fused silica and MD simulations of

water adjacent to a hydrophilic solid surface at increasing distance from the interface.[18] This change is consistent with the molecular coordinate system (Figure 5) and an increasingly negative surface charge with increasing pH, since increases in θ beyond 90° correspond to the hydrogen atoms becoming more aligned at the surface. From this comparison we conclude that the orienting forces felt by each water population are very different. Moreover, if the changes in SFG intensity are due to changes in the average tilt angle than the results suggest the water populations that correspond to the 3200 $cm^{-1}$ mode are flipping their orientation upon increasing the pH from pH 2 to 12, whereas those water molecules that correspond to the 3400 $cm^{-1}$ mode are not.

**Model 2: Change in Degree of Ordering of Water with Varying pH.**

In the above scenario, we have considered a narrow distribution of tilt and twist angles. In reality, these distributions have some width, and it is also likely that the width could change as the interfacial environment changes. We now explore this scenario, where the flipping of water in the diffuse layer is accomplished by a widening of the orientation distribution until the point where it is isotropic when the potential reaches zero, followed by a re-narrowing of the distribution (but with opposite orientation) as the potential increases again with increasing pH, but with opposite sign.

Figure 6G and 6I illustrate that for the 3200 $cm^{-1}$ species at a tilt angle of 150° and a twist angle of 140°, the intensity decreases as the width distribution (σ) increases. This is also consistent with trends in the experimental spectra if the width distribution increases from ~45° with increasing pH until a minimum is reached, at which point the water molecules in the diffuse layer flip, and the intensity again increases but with decreasing σ values, reaching a maximum near zero distribution. For the 3400 $cm^{-1}$ species at a tilt angle of 170° and a twist angle of 55°, the intensity increases with decreasing σ values, reaching maximum intensity at zero width distribution. This is consistent with the monotonic increase in intensity observed in the *pss* spectra, if the width distribution decreases from ~30° towards 0°. Finally, it is worth noting that the plots in Figure 6G, 6H, and 6I are consistent with the dominance of the 3200 versus 3400 $cm^{-1}$ species seen in the experimental SFG data: in the *ssp* and *ppp* polarizations, the 3200 $cm^{-1}$ species has significantly greater intensity than the 3400 $cm^{-1}$ species while in the *pss* scheme, the 3400 $cm^{-1}$ species clearly dominates.

**Possible Molecular Structures of the EDL with Varying pH.**

As mentioned, a method was recently developed using phase-sensitive SFG to reveal the different structures of the double layer (the Stern layer and the diffuse layer) at the air/carboxylic acid film/water interface. In this method the authors described the effective $\chi^{(2)}$ as the sum of a surface contribution ($\chi^{(2)}_{Surface}$) and a diffuse layer contribution, the latter of which was described as a ($\chi^{(3)}$) term that included the interfacial potential as well as a phase factor, which depended on the Debye length.[28] To separate the contributions from these two terms the authors calculated the phase factor and the pH dependence of Φ based on EDL models like the Gouy-Chapman and expected values of the surface charge density of this monolayer as a function of pH. Additionally, the wavenumber dependence of $\chi^{(3)}$ was determined by comparing the spectra at the expected point of zero charge and at low surface charge densities. Subsequently, these values of $\chi^{(3)}$, Φ and the phase factor were used to deconvolute the pH dependent behavior of the surface water from the diffuse layer. In contrast, due to the relatively high ionic strengths used here, in our analysis we are separating the behavior of the water molecules near the surface and in the diffuse layer based on differences in resonant frequency. Moreover, the changes in intensity are considered mainly in terms of changes in the interfacial potential that contribute to the $\chi^{(3)}$ term while changes to $\chi^{(2)}$ for each mode are not considered explicitly. Although considering the intensity changes purely in terms of changes in interfacial potential is undoubtedly an oversimplification of the behavior of water, it provides a useful starting point for understanding the unusual trends in pH for the different spectral regions.

First, we consider what region in the EDL each water population falls. Previously Hore and coworkers' concluded that the 3200 $cm^{-1}$ peak corresponded predominantly to water molecules that were farther from the surface while the 3400 $cm^{-1}$ peak corresponded mainly to water molecules that were closer to the surface based on the greater salt dependence of the former.[18] In support of this interpretation, recent experiments using X-ray photoelectron spectroscopy revealed that the changes of the Stern layer thickness tracked well with the changes in the amplitude of the 3400 $cm^{-1}$ peak in SFG upon increasing electrolyte concentration.[11] Based on these previous studies and the results presented here, we propose that the water in the diffuse part of the EDL (corresponding to 3200 $cm^{-1}$) is flipping orientation with increasing pH while the 3400 $cm^{-1}$ water molecules located close to the surface are not.

We propose different scenarios that could cause this type of behavior at the silica/water interface. The first is similar to that observed on alumina of charge reversal of the interface,[26] except the charge reversal involves the Stern layer overcharging at low pH and high salt concentration instead of the charge on the silica surface reversing sign. Overcharging of the Stern layer occurs when there are more cations in the Stern layer than there are negative surface charges on the silica,[48] causing the Stern layer to have a positive potential ($\Phi_{Stern} > 0$), while the surface maintains a negative potential set up by the siloxides ($\Phi_{Surface} < 0$). As these two potentials influencing the two water populations through the $\chi^{(3)}$ term would be opposite in sign, they would cause the water molecules in the diffuse layer (at 3200 $cm^{-1}$) to adopt the opposite orientation relative to those waters at the silica surface (at 3400 $cm^{-1}$) (Scheme 1A). However as the pH is increased leading to an increase in negative surface sites, the Stern layer would reach a point where the cation concentration equaled the number of surface charges yielding a $\Phi_{Stern}$ of zero, but an even more negative surface potential. This would lead to little order of the diffuse layer waters at 3200 $cm^{-1}$ but significant ordering of the Stern layer waters at 3400 $cm^{-1}$. Further increases in pH would lead to more surface charges than cations in the Stern layer leading to both a negative $\Phi_{Stern}$ and $\Phi_{Surface}$. Over this higher pH range, both water populations would be ordered and orientated in the same direction owing to the same sign of both potentials (Scheme 1B). Although it is commonly assumed that only ions of higher valency can cause charge reversal in the EDL, there is experimental support of this mechanism. Specifically, a change in sign of the zeta potential of silica colloid has been observed with varying pH at high concentrations of monovalent ions such that a positive zeta potential is measured at low pH and a negative potential at high pH.[7-8] (Experimentally the zeta potential is an approximate measure of the Stern layer potential, $\Phi_{Stern}$).[49] In both of the colloidal studies, the point of zero zeta potential was dependent on the concentration of the ions in solution such that as the concentration of ions in-

creased, the pH where the zero zeta potential occurred also shifted to higher pH values. This shift in the zero zeta potential is consistent with the shift in minimum *ssp*-SFG intensity with pH for the 3200 $cm^{-1}$ mode with increasing salt concentration. In contrast, the surface waters at 3400 $cm^{-1}$ exhibited a minimum in the *pss* SFG intensity at pH 2-4 and an increase in intensity with increasing pH, consistent with potentiometric studies that indicate the silica surface becomes more negatively charged upon increasing the pH above 2-3, even in the presence of high salt concentrations.[11] Furthermore, recent nonequilibrium molecular dynamics simulations of electroosmotic flow between parallel slabs of the hydroxylated (110) rutile ($TiO_2$) surface revealed that sodium interacted more than chloride with the surface even at the point of zero charge leading to a positive zeta potential although the rutile surface was net neutral.[50] These simulations are consistent with our observation of aligned water in the diffuse layer even at pH 2-3 when the silica surface is neutral, which could be due to stronger interactions of sodium than chloride with the neutral silica.

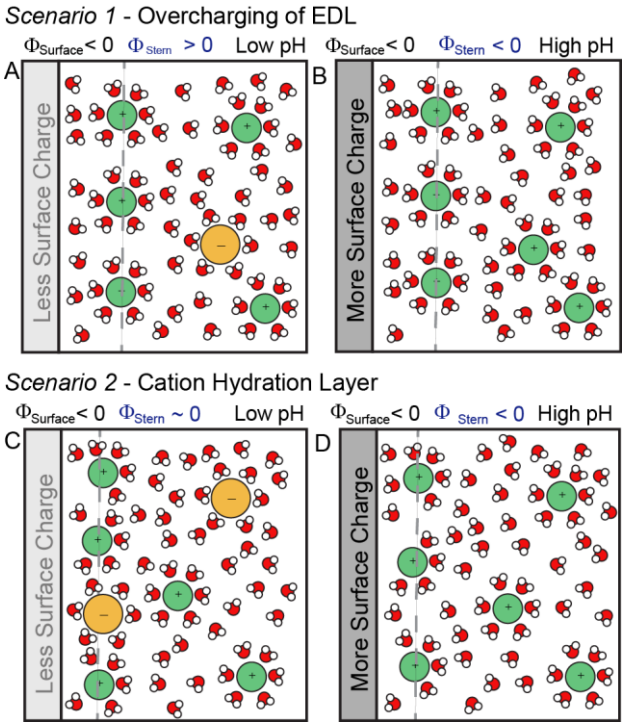


**Scheme 1.** Potential structures of the EDL that describe the behavior observed in the SFG intensity. Scenario 1 involves the overcharging of the EDL at low pH (A) and high pH (B). Scenario two depicts the cation hydration layer contributing to the SFG at low pH (C) and high pH (D).

The interactions described by the $\chi^{(3)}$ term assume the potentials acting on the water in the Stern layer or diffuse layer lead to alignment of the dipole moment of water with the surface normal (corresponding to a tilt angle of 0° or 180° depending on the sign of the potential). Accordingly, this overcharging scenario is consistent with the molecular model proposed above. For the waters contributing at 3200 $cm^{-1}$, the assembly begins with a tilt angle nearer 0° at low pH owing to the positive Stern layer potential. This corresponds to the oxygen atoms pointing towards the surface (refer to Figure 5). The tilt angle then systematically increases with increasing pH until it passes through 90° (corresponding to a zero Stern layer potential) and then approaches 180° at higher pH when the Stern layer potential is large in magnitude and negative. As a result of this flip in orientation, the hydrogen atoms are instead pointed towards the surface, which is consistent with the increased negative charge on the silica surface at high pH. In contrast, for 3400 $cm^{-1}$ the dipole moment becomes more aligned with the surface normal with increasing pH as the surface potential goes from zero to large negative values, consistent with the systematic increase in the tilt angle with pH above 90° toward 180°. This means that water molecules closer to the interface have their oxygen atoms pointing away from the surface at low pH.

The second scenario involves the distortion of the hydration layer around the ions at high electrolyte concentrations. If the $Na^+$ ions in the Stern layer specifically absorb at the interface, then the hydration layer around the ion could become distorted (Scheme 1C and 1D). In this case, the water molecules in the hydration layer could contribute to the $\chi^{(2)}$ signal owing to their lack of centrosymmetry. Moreover, due to partial dehydration these waters would be mainly orientated with the oxygen towards the surface owing to the positive charge of the $Na^+$. This dehydration of the $Na^+$ ion at the silica surface has been previously predicted by simulations at high concentrations.[47] Alternatively, an outer sphere complex could form between the sodium and the surface (i.e., a water in the cation hydration layer could directly hydrogen bond to the surface), which would also break the symmetry of the hydration shell leading to SFG. The formation of such an outer sphere complex was proposed for the silica interface in the presence of 100 mM NaCl and pH 10 in the XPS surface potential study on silica colloids.

If the resonant frequencies of the diffuse layer water and this cation hydration layer are close, there would be a cancellation of signal. Water in the $Na^+$ hydration layer has been proposed to resonate at 3150 $cm^{-1}$,[51] which should interfere with the 3200 $cm^{-1}$ mode. Another way of describing this is to consider that the hydration layer contributes to the $\chi^{(2)}_{3200}$ term, which interferes with the $\chi^{(3)}_{3200}$ response of water in the diffuse layer polarized by the Stern layer potential ($\Phi_{Stern}$). Additionally, the lower wavenumber of the hydration layer dominating at low pH is consistent with the red shift we see in the *ssp*-SFG spectra upon passing through the minimum in intensity with decreasing pH (Figure 2A and Figure 3A). The minimum observed in the SFG would then correspond to the pH where the most cancellation between the water molecules in the hydration layer and the water molecules aligned by the negative Stern layer potential in the diffuse layer. As the pH is further decreased beyond this pH, the Stern layer potential should be come smaller (if it does not overcharge). Hence, the water molecules from the hydration layer would begin to dominate the SFG signal leading to an overall increase in intensity (Scheme 1C). At higher pH, the magnitude of the surface potential ($\Phi_{Stern} < 0$) is able to align a large number of water molecules in the diffuse layer, which should dominate the SFG spectra compared to the water molecules in the hydration layers leading once again to increasing signal intensity with increasing pH (Scheme 1D). In this scenario, the pH value of the minimum would also shift with electrolyte concentration because the higher electrolyte concentration should lead to thinner diffuse layers owing to the decrease in the Debye length with increasing salt concentration. As such, optimal cancellation of the hydrated cation and diffuse layer water populations would occur at a higher pH in the presence of high salt concentrations.

It is possible that both scenarios are contributing. Indeed, the presence of signal intensity at 3200 $cm^{-1}$ at the minimum in the *ssp* and *ppp*-SFG (Figures 2A and 3A) indicates that

there is some structured water at all pH, which would be consistent with some alignment of waters in the low wavenumber region that do not depend directly on the Stern layer potential. Both scenarios suggest that the net assembly of waters in the ~3200 $cm^{-1}$ mode flip orientation (either because of a change in the Stern layer potential or because the hydrated cation waters outnumber the diffuse layer waters), which agree with two phase-sensitive SFG experiments performed at the silica/water interface at low salt concentration. These phase-sensitive measurements performed over the same pH range (pH 2-12) on silica revealed that the waters contributing in the low wavenumber range on average flipped orientation while those contributing to the mode at higher wavenumber did not.[45, 52] The authors attributed this flip to different hydrogen-bonding structures at the silica surface with changing pH, in contrast to our model where the water flipping is proposed to occur away from the silica immediately outside the Stern layer or in the diffuse layer.

Finally, another possibility for the origin of the signal intensity at the minimum is interference between the non-resonant $\chi^{(2)}$ response of the interface ($\chi^{(2)}_{NR}$) and the field-dependent $\chi^{(3)}$ terms. Future work is aimed at quantifying the field dependence of the water response and comparing it with surface potential measurements to disentangle the different contributions to the signal intensity.

## CONCLUSION

Vibrational SFG spectroscopic studies suggested that different polarization combinations probe the structure and behavior of water within different regions of the EDL in response to changes in both electrolyte concentration and pH. The data suggest that the observed 3200 $cm^{-1}$ peak probes water molecules further from the surface in the diffuse layer of the EDL, whereas the 3400 $cm^{-1}$ peak probes water molecules in the Stern layer. In addition, our results show that the 3200 $cm^{-1}$ peak (diffuse layer) can be probed with either *ssp* or *ppp* polarization combinations, while the 3400 $cm^{-1}$ peak can be probed using *pss* polarization combination. Most strikingly, we observe that the orienting forces acting on each water population are very different upon varying the pH in the presence of high salt concentrations. Our results are consistent with the presence of oriented water, even at low pH near the point-of-zero charge of silica. This oriented water is due to water oriented further from the surface, either owing to interactions with cations at the surface or a positive potential arising from overcharging of the EDL. These results have a significant impact on previous interpretations of high electrolyte concentration data in non-linear optical experiments as they reinforce that different water populations can reside in very different proximity to the surface and accordingly experience different local environments based on the formation of the Stern layer.

## EXPERIMENTAL SECTION

### Sum Frequency Generation (SFG)

Two different SFG configurations were used in this study. Broadband (fs) and scanning (ps) SFG, both of which are described in detail in the supporting information. In general, a tunable IR laser (either fs or ps) is overlapped in time and space with a visible laser (typically ps) at the silica/water interface. The sum of the two lasers was reflected from the surface and passed through a filter to remove the residual fundamental beams. The magnitude of the output light was then measured. Multiple polarization combinations were used in the collection of the data, for example, *ssp*-SFG corresponds to *s*-polarized sum frequency, *s*-polarized visible, and *p*-polarized IR.

### Sample Preparation

An IR-grade fused silica sample (hemisphere or prism) was first sonicated in ultra-pure water (18 MΩ). The sample was then sonicated in methanol and then rinsed with ultra-pure water. This was followed by sonication and rinses with ultra-pure water. The silica sample was then immersed in a piranha solution (3:1 mixture of concentrated sulfuric acid: 30% hydrogen peroxide) for 1 hour. The sample was then rinsed with copious amount of ultra-pure water to ensure no piranha solution remained. The sample was then sonicated and rinsed for four more times with ultra-pure water. After rinsing, the sample was then placed in an oven at 100°C for 30 min, then the sample was allowed to cool to room temperature. This was then followed by plasma cleaning in air for 2 min. The sample was immediately used in an experiment.

### SFG Titrations

To start, the silica sample was exposed to ultra-pure water and SFG was gathered. Next, the water was removed from the sample cell, and salt solution (either 500, 100 or 10 mM) was added to the sample cell. The salt solution was allowed to equilibrate with the interface for 30 min and the spectra were gathered. The pH of the solution was adjusted with HCl or NaOH that was dissolved in the salt solution of interest (i.e. if the titration was done at 500 mM NaCl, then HCl or NaOH was prepared in a 500 mM NaCl solution). After each pH adjustment the sample was equilibrated for 5 min and then the spectra were taken at each IR setting and the pH of the solution measured. The titrations were conducted from pH 6 to 12 or from pH 7 to 2 to avoid hysteresis due to extreme pH seen in previous SHG experiments.[53]

### Spectral Intensity Simulations

It is customary to model the SFG intensity for specific vibrational modes by projecting the relevant hyperpolarizability tensor elements $\alpha^{(2)}_{lmn}$ into the laboratory frame to yield $\alpha^{(2)}_{ijk}$ according to the experimental polarization scheme of interest. Here *l,m,n* are any of the molecular-frame Cartesian coordinates *a*, *b* or *c*, and *i,j,k* are any of the lab frame Cartesian coordinates *x*, *y*, *z* where the silica–water surface is in the *xy* plane, and *z* is the outward pointing surface normal. The ensemble of $\alpha^{(2)}_{ijk}$ values for each vibrational mode then yields $\chi^{(2)}_{ijk}$, whose magnitude squared is proportional to the measured SFG intensity. This method has been successfully applied to many small molecules.[54-57] However, when it comes to liquid water, the situation is considerably more complicated on account of the multitude of hydrogen bonding interactions that result in coupled OH oscillators spanning a nearly 1000 $cm^{-1}$ frequency range in the 2800–3800 $cm^{-1}$ window.

One approach to address this complexity is to use atomistic molecular dynamics simulations combined with electronic structure calculations to generate $\alpha^{(2)}_{lmn}$ profiles of water molecules from a scheme that couples two OH oscillators based on the net force along each of the OH bonds. In this way, the environment at the surface is taken into account. Such a scheme was originally proposed by Morita and Hynes[42] and applied to modeling the SFG spectra at the air–water surface. Roy *et al.* later applied the same method to study water next to model hydrophilic and hydrophobic surfaces, and produced results that qualitatively matched experimental spectra, accounting for the lack of free OH modes at hydrophilic surfaces.[58] Here we use data from those simulations on hydrophilic OH-terminated surfaces to extract $\alpha^{(2)}_{lmn}$ for interfacial water

molecules. The overall goal is to arrive at the hyperpolarizability for a typical 3200 $cm^{-1}$ species, and also for a 3400 $cm^{-1}$ species that takes the vibrational mode symmetry, strength of the hydrogen bonding network, and coordination into account. The general scheme is to determine the frequency of each OH oscillator according to the force projected along the OH bond. Details of the molecular dynamics simulations and the preparation of the surfaces have been described previously.[58] From the two uncoupled frequencies $\omega_1$ and $\omega_2$ of each water molecule, we determine the eigenvalues $\omega_{high}$ and $\omega_{low}$ and corresponding eigenvector

$$v_{low} = \begin{bmatrix} c_1 \\ c_2 \end{bmatrix}_{low}, v_{high} = \begin{bmatrix} c_1 \\ c_2 \end{bmatrix}_{high}$$

$$v_{low} = \begin{bmatrix} c_1 \\ c_2 \end{bmatrix}_{low}, v_{high} = \begin{bmatrix} c_1 \\ c_2 \end{bmatrix}_{high}$$

of the matrix

$$A = \begin{bmatrix} \omega_1 & V_{1,2} \\ V_{1,2} & \omega_2 \end{bmatrix}$$

such that

$$v_{low} \cdot A = \omega_{low} \cdot v_{low}$$

$$v_{high} \cdot A = \omega_{high} \cdot v_{high}$$

where $v_{1,2}$=49.5 $cm^{-1}$ is the midpoint between the gas-phase symmetric and anti-symmetric frequencies. These coupling constants are then used to obtain the water molecule polarizability and dipole moment derivatives as a function of vibrational mode frequency.

$$\frac{\partial \alpha_{ij}^{(1)}}{\partial Q} = c_1 \cdot R(\theta_1,\varphi_1,\psi_1)^T \cdot \frac{\partial \alpha_{lm}^{(1)}}{\partial r_1} \cdot R(\theta_1,\varphi_1,\psi_1) + c_2 \cdot R(\theta_2,\varphi_2,\psi_2)^T \cdot \frac{\partial \alpha_{lm}^{(1)}}{\partial r_2} \cdot R(\theta_2,\varphi_2,\psi_2)$$

$$\frac{\partial \mu_k}{\partial Q} = c_1 \cdot \frac{\partial \mu_n}{\partial r_1} \cdot R(\theta_1,\varphi_1,\psi_1) + c_2 \cdot \frac{\partial \mu_n}{\partial r_2} \cdot R(\theta_2,\varphi_2,\psi_2)$$

where θ, φ, and ψ are the Euler angles that rotate each of the O–H bonds ($r_1$ and $r_2$) into the lab frame via the transformation operator **R** whose elements are the scalar product of the unit vectors in the molecular *l,m,n* axes and the lab frame *i,j,k* axes. Values of the dipole moment and polarizability derivatives along the bond axis $r_1$ are taken from Morita and Hynes.[42] Any of the 27 elements of the hyperpolarizability tensor may now be obtained according to

$$\alpha_{ijk}^{(2)}(\omega_{IR}) \approx \frac{1}{2m\omega_{low}} \left[ \frac{\alpha_{ij}^{(1)}}{\partial Q} \cdot \frac{\mu_k}{\partial Q} \right]_{low} \frac{1}{\omega_{low} - \omega_{IR} - i\Gamma} + \frac{1}{2m\omega_{high}} \left[ \frac{\alpha_{ij}^{(1)}}{\partial Q} \cdot \frac{\mu_k}{\partial Q} \right]_{high} \frac{1}{\omega_{high} - \omega_{IR} - i\Gamma}$$

This allows for spectral interference between modes existing at all values of $\omega_{IR}$. The final step is to select an average value of $\alpha^{(2)}$ from a narrow band within the 3200 $cm^{-1}$ and 3400 $cm^{-1}$ region, project them in the plane of the silica surface according to the polarization scheme of interest. We model the three measured experimental spectral intensities according to

$$I_{ssp} = \left| L_{yy} e_y \cdot \alpha_{yyz}^{(2)} \cdot L_{yy} e_y \cdot L_{zz} e_z \right|^2$$

$$I_{sps} = \left| L_{yy} e_y \cdot \alpha_{yzy}^{(2)} \cdot L_{zz} e_z \cdot L_{yy} e_y \right|^2$$

$$I_{ppp} = \left| L_{xx} e_x \times \alpha_{xxz}^{(2)} \times L_{xx} e_x \times L_{zz} e_z + L_{xx} e_x \times \alpha_{xzx}^{(2)} \times L_{zz} e_z \times L_{xx} e_x + L_{zz} e_z \times \alpha_{zxx}^{(2)} \times L_{xx} e_x \times L_{xx} e_x + L_{zz} e_z \times \alpha_{zzz}^{(2)} \times L_{zz} e_z \times L_{zz} e_z \right|^2$$

where the macroscopic local field corrections $L_{ii}$ and unit polarization vectors $e_i$ are defined according to the angle of incidence, and frequency-dependent wavelength of water and silica. Expressions for these terms are given elsewhere.[57, 59] Their evaluation required refractive index dispersion data for water[60] and silica.[61]

In the final step, the model 3200 $cm^{-1}$ and 3400 $cm^{-1}$ intensities are calculated according to hypothetical tilt θ and twist ψ distributions, assuming a uniform distribution of the azimuthal angle ϕ in the plane of the surface. Such quantities are obtained by the additional coordinate transformation

$$\alpha_{i'j'k'}^{(2)}(\theta_0,\sigma_\theta,\psi_0,\sigma_\psi) = \sum_{\alpha}^{x,y,z} \sum_{\beta}^{x,y,z} \sum_{\gamma}^{x,y,z} \int_0^{2\pi} \int_0^{\pi} R_{i,i'}(\theta,\psi) \cdot R_{j,j'}(\theta,\psi) \times R_{k,k'}(\theta,\psi) \cdot \alpha_{ijk}^{(2)}(\theta,\psi) \cdot f(\theta,\psi;\theta_0,\sigma_\theta,\psi_0,\sigma_\psi) \sin\theta d\theta d\psi$$

where *f* is the orientation distribution function. The top row of Figure 6 illustrates the results obtained for the 3200 $cm^{-1}$ species for an infinitely narrow distribution of tilt and twist angles

$$f(\theta,\psi;\theta_0,\sigma_\theta,\psi_0,\sigma_\psi) = \delta(\theta-\theta_0,\psi-\psi_0)$$

where the variation in SFG intensity is plotted as a function of $\theta_0$ along the horizontal, and $\psi_0$ along the vertical axes. We have then considered the possibility of the mean tilt and twist angles fixed at ($\theta_0$=45°, $\psi_0$=40°) and plotted the variation in SFG intensity as a function of the width σ assuming $\sigma_\theta=\sigma_\psi$ and a Gaussian distribution function

$$f(\theta,\psi;\theta_0,\sigma_\theta,\psi_0,\sigma_\psi) = \exp\left[ -\frac{(\theta-\theta_0)^2}{2\sigma_\theta^2} - \frac{(\psi-\psi_0)^2}{2\sigma_\psi^2} \right]$$

as illustrated in the bottom row of Figure 6, plotted in orange for the 3200 $cm^{-1}$ species. Considering values of ($\theta_0$=50°, $\psi_0$=30°) for the 3400 $cm^{-1}$ species resulted in the blue lines indicating SFG intensity as a function of σ.

## ASSOCIATED CONTENT

Supporting Information. Detailed descriptions of both laser setups used in the experiments are given. The broadband *ssp*-SFG titrations for 10, 100, and 500 mM NaCl are shown. In addition, a comparison of the integrated intensity for 500 mM NaCl between the broadband (fs) and scanning (ps) SFG systems is presented. This material is available free of charge via the Internet at http://pubs.acs.org.

## AUTHOR INFORMATION

### Corresponding Author

* Julianne Gibbs (julianne.gibbs@ualberta.ca), *Dennis Hore (dkhore@uvic.ca)

## ACKNOWLEDGMENT

JMG acknowledges the Institute of Oil Sands Innovation (IOSI 2012-06), Petro Canada for a Young Innovator Award and the Sloan Foundation. JMG and DKH acknowledge Natural Science and Engineering Research Centre Discovery Grant. AMD acknowledges an Alberta Innovates Technology Futures graduate fellowship. SK acknowledges Alberta/Technical University of Munich International Graduate School for Hybrid Functional Materials (ATUMS).

We gratefully acknowledge helpful discussions with Dr. Matthew Brown (ETH), Prof. Eric Tyrode (KTH), and Prof. Hongfei Wang (PNNL).

## ABBREVIATIONS

EDL = electric double layer, XPS = X-ray photoelectron spectroscopy, SFG = sum frequency generation.

## REFERENCES


1. Chapman, D. L., A Contribution to the Theory of Electrocapillarity. *Philos. Mag. Series 6* **1913**, *25*, 475-481.
2. Grahame, D. C., The Electrical Double Layer and the Theory of Electrocapillarity. *Chem. Rev.* **1947**, *41*, 441-501.
3. Bockris, J. O. M.; Devanathan, M. A. V.; Muller, K., On the Structure of Charged Interfaces. *P. Roy. Soc. A - Math. Phy.* **1963**, *274*, 55-79.
4. Stern, O., *Z. Elektrochem.* **1924**, *30*, 508-516.
5. Karlsson, M.; Craven, C.; Dove, P.; Casey, W., Surface Charge Concentrations on Silica in Different 1.0 M Metal-Chloride Background Electrolytes and Implications for Dissolution Rates. *Aquat. Geochem.* **2001**, *7*, 13-32.
6. Dove, P. M.; Craven, C. M., Surface Charge Density on Silica in Alkali and Alkaline Earth Chloride Electrolyte Solutions. *Geochim. Cosmochim. Acta.* **2005**, *69*, 4963-4970.
7. Kosmulski, M., Positive Electrokinetic Charge of Silica in the Presence of Chlorides. *J. Coll. Interf. Sci.* **1998**, *208*, 543-545.
8. Franks, G. V., Zeta Potentials and Yield Stresses of Silica Suspensions in Concentrated Monovalent Electrolytes: Isoelectric Point Shift and Additional Attraction. *J. Coll. Interf. Sci.* **2002**, *249*, 44-51.
9. Gmür, T. A.; Goel, A.; Brown, M. A., Quantifying Specific Ion Effects on the Surface Potential and Charge Density at Silica Nanoparticle–Aqueous Electrolyte Interfaces. *J. Phys. Chem. C* **2016**, *120*, 16617-16625.
10. Brown, M. A.; Abbas, Z.; Kleibert, A.; Green, R. G.; Goel, A.; May, S.; Squires, T. M., Determination of Surface Potential and Electrical Double-Layer Structure at the Aqueous Electrolyte-Nanoparticle Interface. *Phys.Rev. X* **2016**, *6*, 011007.
11. Brown, M. A.; Goel, A.; Abbas, Z., Effect of Electrolyte Concentration on the Stern Layer Thickness at a Charged Interface. *Angew. Chem. Int. Ed.* **2016**, *55*, 3790-3794.
12. Nihonyanagi, S.; Yamaguchi, S.; Tahara, T., Direct Evidence for Orientational Flip-Flop of Water Molecules at Charged Interfaces: A Heterodyne-Detected Vibrational Sum Frequency Generation Study. *J. Chem. Phys.* **2009**, *130*, 204704.
13. Nihonyanagi, S.; Yamaguchi, S.; Tahara, T., Water Hydrogen Bond Structure near Highly Charged Interfaces Is Not Like Ice. *J. Am. Chem. Soc.* **2010**, *132*, 6867-6869.
14. Verreault, D.; Hua, W.; Allen, H. C., From Conventional to Phase-Sensitive Vibrational Sum Frequency Generation Spectroscopy: Probing Water Organization at Aqueous Interfaces. *J. Phys. Chem. Lett.* **2012**, *3*, 3012-3028.
15. Livingstone, R. A.; Nagata, Y.; Bonn, M.; Backus, E. H. G., Two Types of Water at the Water–Surfactant Interface Revealed by Time-Resolved Vibrational Spectroscopy. *J. Am. Chem. Soc.* **2015**, *137*, 14912-14919.
16. Du, Q.; Freysz, E.; Shen, Y. R., Vibrational Spectra of Water Molecules at Quartz/Water Interfaces. *Phys. Rev. Lett.* **1994**, *72*, 238-241.
17. Ostroverkhov, V.; Waychunas, G. A.; Shen, Y. R., Vibrational Spectra of Water at Water/A-Quartz (0001) Interface. *Chem. Phys. Lett.* **2004**, *386*, 144-148.
18. Jena, K. C.; Hore, D. K., Variation of Ionic Strength Reveals the Interfacial Water Structure at a Charged Mineral Surface. *J. Phys. Chem. C* **2009**, *113*, 15364-15372.
19. Jena, K. C.; Covert, P. A.; Hore, D. K., The Effect of Salt on the Water Structure at a Charged Solid Surface: Differentiating Second- and Third-Order Nonlinear Contributions. *J. Phys. Chem. Lett.* **2011**, *2*, 1056-1061.
20. Covert, P. A.; Jena, K. C.; Hore, D. K., Throwing Salt into the Mix: Altering Interfacial Water Structure by Electrolyte Addition. *J. Phys. Chem. Lett.* **2013**, *5*, 143-148.
21. Covert, P. A.; Hore, D. K., Geochemical Insight from Nonlinear Optical Studies of Mineral–Water Interfaces. *Annu. Rev. Phys. Chem.* **2016**, *67*, 233-257.
22. Dewan, S.; Yeganeh, M. S.; Borguet, E., Experimental Correlation between Interfacial Water Structure and Mineral Reactivity. *J. Phys. Chem. Lett.* **2013**, *4*, 1977-1982.
23. Yang, Z.; Li, Q.; Chou, K. C., Structures of Water Molecules at the Interfaces of Aqueous Salt Solutions and Silica: Cation Effects. *J. Phys. Chem. C* **2009**, *113*, 8201-8205.
24. Dalstein, L.; Potapova, E.; Tyrode, E., The Elusive Silica/Water Interface: Isolated Silanols under Water as Revealed by Vibrational Sum Frequency Spectroscopy. *Phys. Chem. Chem. Phys.* **2017**.
25. Sung, J.; Zhang, L.; Tian, C.; Shen, Y. R.; Waychunas, G. A., Effect of Ph on the Water/A-Al2o3 ($1\bar{1}02$) Interface Structure Studied by Sum-Frequency Vibrational Spectroscopy. *J. Phys. Chem. C* **2011**, *115*, 13887-13893.
26. Yeganeh, M. S.; Dougal, S. M.; Pink, H. S., Vibrational Spectroscopy of Water at Liquid/Solid Interfaces: Crossing the Isoelectric Point of a Solid Surface. *Phys. Rev. Lett.* **1999**, *83*, 1179-1182.
27. Tuladhar, A.; Piontek, S. M.; Borguet, E., Insights on Interfacial Structure, Dynamics, and Proton Transfer from Ultrafast Vibrational Sum Frequency Generation Spectroscopy of the Alumina(0001)/Water Interface. *J. Phys. Chem. C* **2017**, *121*, 5168-5177.
28. Wen, Y.-C.; Zha, S.; Liu, X.; Yang, S.; Guo, P.; Shi, G.; Fang, H.; Shen, Y. R.; Tian, C., Unveiling Microscopic Structures of Charged Water Interfaces by Surface-Specific Vibrational Spectroscopy. *Phys. Rev. Lett.* **2016**, *116*, 016101.
29. Scheu, R.; Chen, Y.; Subinya, M.; Roke, S., Stern Layer Formation Induced by Hydrophobic Interactions: A Molecular Level Study. *J. Am. Chem. Soc.* **2013**, *135*, 19330-19335.
30. Lovering, K. A.; Bertram, A. K.; Chou, K. C., New Information on the Ion-Identity-Dependent Structure of Stern Layer Revealed by Sum Frequency Generation Vibrational Spectroscopy. *J. Phys. Chem. C* **2016**, *120*, 18099-18104.
31. Gonella, G.; Lütgebaucks, C.; de Beer, A. G. F.; Roke, S., Second Harmonic and Sum-Frequency Generation from Aqueous Interfaces Is Modulated by Interference. *J. Phys. Chem. C* **2016**, *120*, 9165-9173.
32. Ohno, P. E.; Saslow, S. A.; Wang, H.-f.; Geiger, F. M.; Eisenthal, K. B., Phase-Referenced Nonlinear Spectroscopy of the A-Quartz/Water Interface. *Nature Commun.* **2016**, *7*, 13587.
33. Shen, Y. R., Surface Properties Probed by Second-Harmonic and Sum-Frequency Generation. *Nature* **1989**, *337*, 519-525.
34. Lambert, A. G.; Davies, P. B.; Neivandt, D. J., Implementing the Theory of Sum Frequency Generation Vibrational Spectroscopy: A Tutorial Review. *Appl. Spectrosc. Rev.* **2005**, *40*, 103-145.

35. Boyd, R. W., *Nonlinear Optics*; Academic Press: San Diego, California, 1992.
36. Iler, R. K., *The Chemistry of Silica.*; John Wiley & Sons, Inc.: United States of America, 1979.
37. Ong, S.; Zhao, X.; Eisenthal, K. B., Polarization of Water Molecules at a Charged Interface: Second Harmonic Studies of the Silica/Water Interface. *Chem. Phys. Lett.* **1992**, *191*, 327-335.
38. Gragson, D. E.; McCarty, B. M.; Richmond, G. L., Ordering of Interfacial Water Molecules at the Charged Air/Water Interface Observed by Vibrational Sum Frequency Generation. *J. Am. Chem. Soc.* **1997**, *119*, 6144-6152.
39. Valleau, J. P.; Torrie, G. M., The Electrical Double Layer. Iii. Modified Gouy−Chapman Theory with Unequal Ion Sizes. *J. Chem. Phys.* **1982**, *76*, 4623-4630.
40. Sovago, M.; Campen, R. K.; Wurpel, G. W. H.; Müller, M.; Bakker, H. J.; Bonn, M., Vibrational Response of Hydrogen-Bonded Interfacial Water Is Dominated by Intramolecular Coupling. *Phys. Rev. Lett.* **2008**, *100*, 173901.
41. Tyrode, E.; Liljeblad, J. F. D., Water Structure Next to Ordered and Disordered Hydrophobic Silane Monolayers: A Vibrational Sum Frequency Spectroscopy Study. *J. Phys. Chem. C* **2013**, *117*, 1780-1790.
42. Morita, A.; Hynes, J. T., A Theoretical Analysis of the Sum Frequency Generation Spectrum of the Water Surface. *Chem. Phys.* **2000**, *258*, 371-390.
43. Liu, D.; Ma, G.; Levering, L. M.; Allen, H. C., Vibrational Spectroscopy of Aqueous Sodium Halide Solutions and Air−Liquid Interfaces: Observation of Increased Interfacial Depth. *J. Phys. Chem. B* **2004**, *108*, 2252-2260.
44. Gan, W.; Wu, D.; Zhang, Z.; Feng, R.-r.; Wang, H.-f., Polarization and Experimental Configuration Analyses of Sum Frequency Generation Vibrational Spectra, Structure, and Orientational Motion of the Air/Water Interface. *J. Chem. Phys.* **2006**, *124*, 114705.
45. Myalitsin, A.; Urashima, S.-h.; Nihonyanagi, S.; Yamaguchi, S.; Tahara, T., Water Structure at the Buried Silica/Aqueous Interface Studied by Heterodyne-Detected Vibrational Sum-Frequency Generation. *J. Phys. Chem. C* **2016**, *120*, 9357-9363.
46. Trudeau, T. G.; Jena, K. C.; Hore, D. K., Water Structure at Solid Surfaces of Varying Hydrophobicity. *J. Phys. Chem. C* **2009**, *113*, 20002-20008.
47. Dewan, S.; Carnevale, V.; Bankura, A.; Eftekhari-Bafrooei, A.; Fiorin, G.; Klein, M. L.; Borguet, E., Structure of Water at Charged Interfaces: A Molecular Dynamics Study. *Langmuir* **2014**, *30*, 8056-8065.
48. Lyklema, J., Overcharging, Charge Reversal: Chemistry or Physics? *Colloid. Surface. A.* **2006**, *291*, 3-12.
49. Lyklema, J., Colloidal Models. A Bit of History. *J. Coll. Interf. Sci.* **2015**, *446*, 308-316.
50. Předota, M.; Machesky, M. L.; Wesolowski, D. J., Molecular Origins of the Zeta Potential. *Langmuir* **2016**, *32*, 10189-10198.
51. Schultz, Z. D.; Shaw, S. K.; Gewirth, A. A., Potential Dependent Organization of Water at the Electrified Metal−Liquid Interface. *J. Am. Chem. Soc.* **2005**, *127*, 15916-15922.
52. Ostroverkhov, V.; Waychunas, G. A.; Shen, Y. R., New Information on Water Interfacial Structure Revealed by Phase-Sensitive Surface Spectroscopy. *Phys. Rev. Lett.* **2005**, *94*, 046102.
53. Darlington, A. M.; Gibbs-Davis, J. M., Bimodal or Trimodal? The Influence of Starting Ph on Site Identity and Distribution at the Low Salt Aqueous/Silica Interface. *J. Phys. Chem. C* **2015**, *119*, 16560-16567.
54. Chase, H. M.; Chen, S.; Fu, L.; Alice Upshur, M.; Rudshteyn, B.; Thomson, R. J.; Wang, H.-F.; Batista, V. S.; Geiger, F. M., Orientations of Nonlocal Vibrational Modes from Combined Experimental and Theoretical Sum Frequency Spectroscopy. *Chem. Phys. Lett.*
55. Hall, S. A.; Jena, K. C.; Covert, P. A.; Roy, S.; Trudeau, T. G.; Hore, D. K., Molecular-Level Surface Structure from Nonlinear Vibrational Spectroscopy Combined with Simulations. *J. Phys. Chem. B* **2014**, *118*, 5617-5636.
56. Wang , H.-F.; Gan, W.; Lu, R.; Rao, Y.; Wu, B.-H., Quantitative Spectral and Orientational Analysis in Surface Sum Frequency Generation Vibrational Spectroscopy. *Int. Rev. Phys. Chem.* **2005**, *24*, 191-256.
57. Wang, H.-F.; Velarde, L.; Gan, W.; Fu, L., Quantitative Sum-Frequency Generation Vibrational Spectroscopy of Molecular Surfaces and Interfaces: Lineshape, Polarization, and Orientation. *Annu. Rev. Phys. Chem.* **2015**, *66*, 189-216.
58. Roy, S.; Hore, D. K., Simulated Structure and Nonlinear Vibrational Spectra of Water Next to Hydrophobic and Hydrophilic Solid Surfaces. *J. Phys. Chem. C* **2012**, *116*, 22867-22877.
59. Liljeblad, J. F. D.; Tyrode, E., Vibrational Sum Frequency Spectroscopy Studies at Solid/Liquid Interfaces: Influence of the Experimental Geometry in the Spectral Shape and Enhancement. *J. Phys. Chem. C* **2012**, *116*, 22893-22903.
60. Segelstein, D. J. The Complex Refractive Index of Water. Master's Thesis. University of Missouri, Kansas City, 1981.
61. Malitson, I. H., Interspecimen Comparison of the Refractive Index of Fused Silica. *J. Opt. Soc. Am.* **1965**, *55*, 1205-1209.


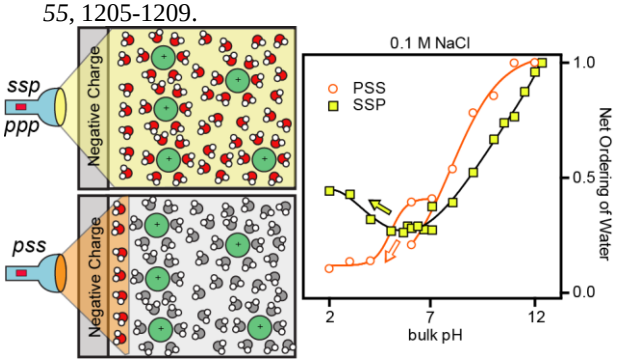

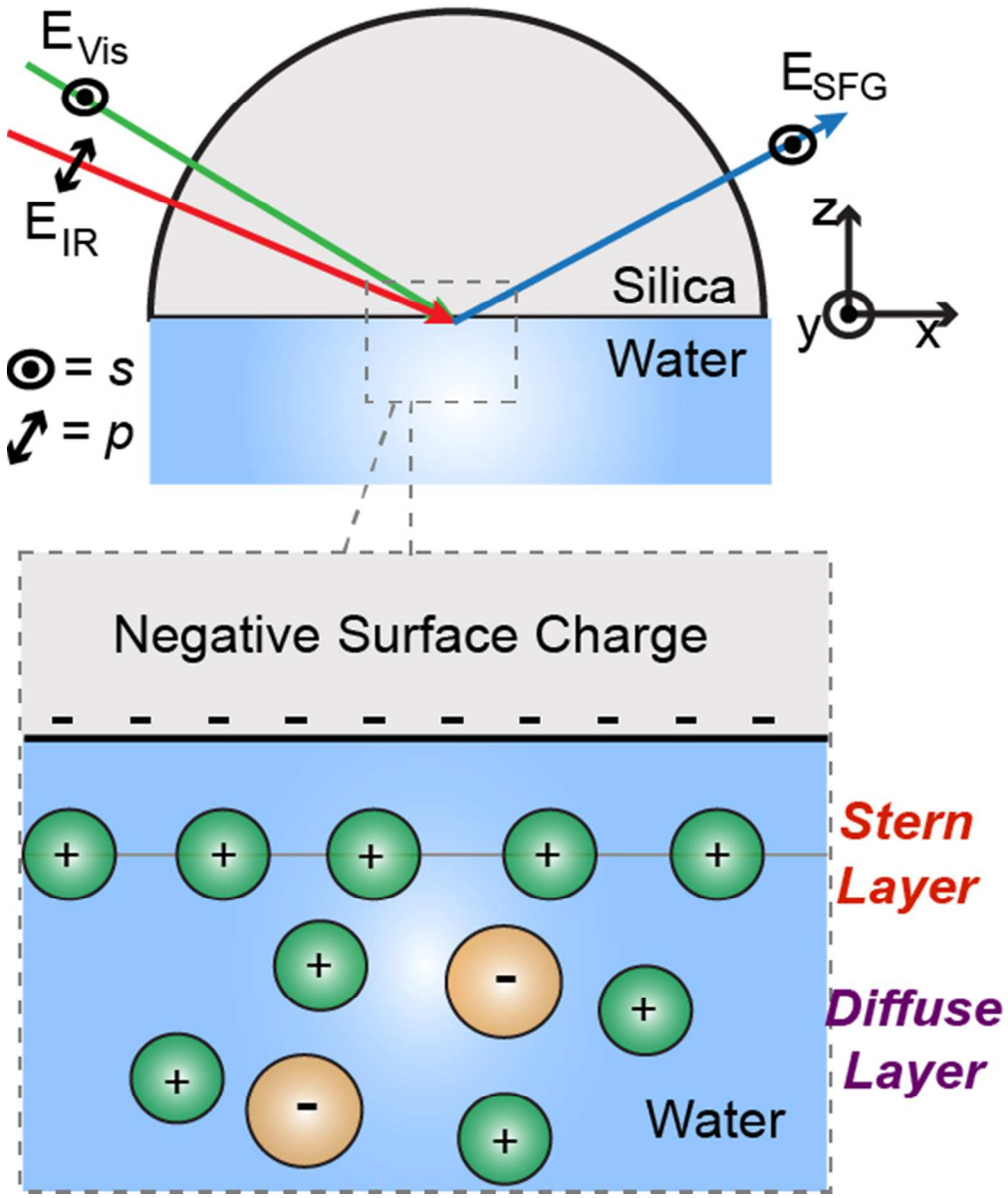


49x59mm (300 x 300 DPI)

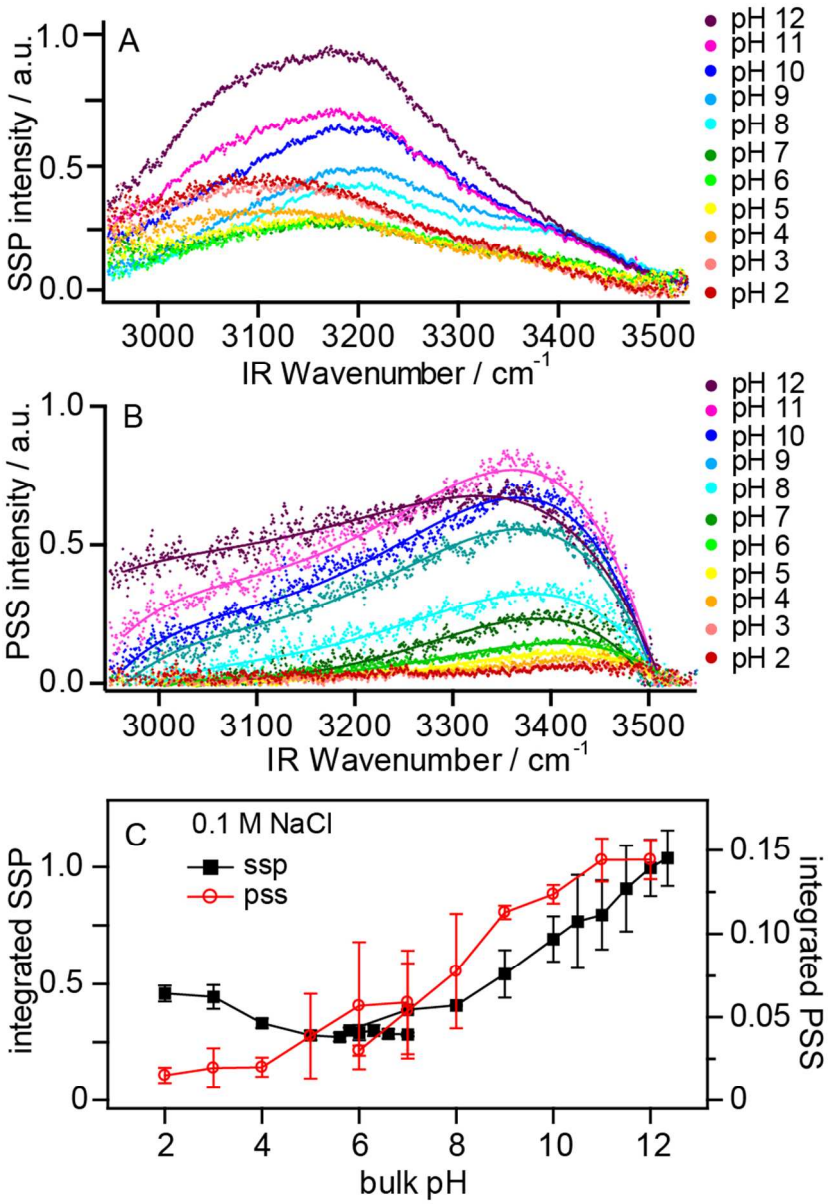


80x117mm (300 x 300 DPI)

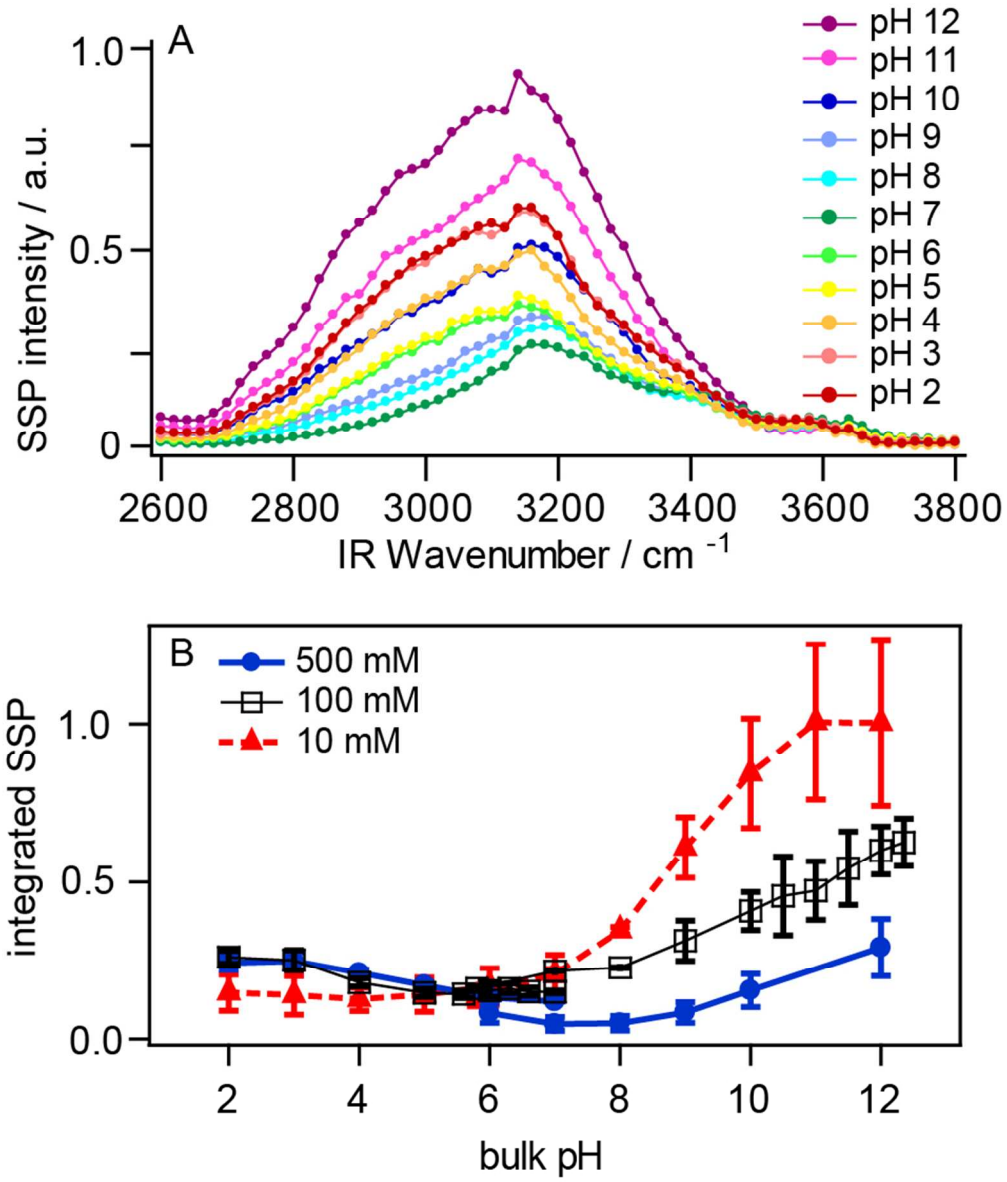


80x94mm (300 x 300 DPI)

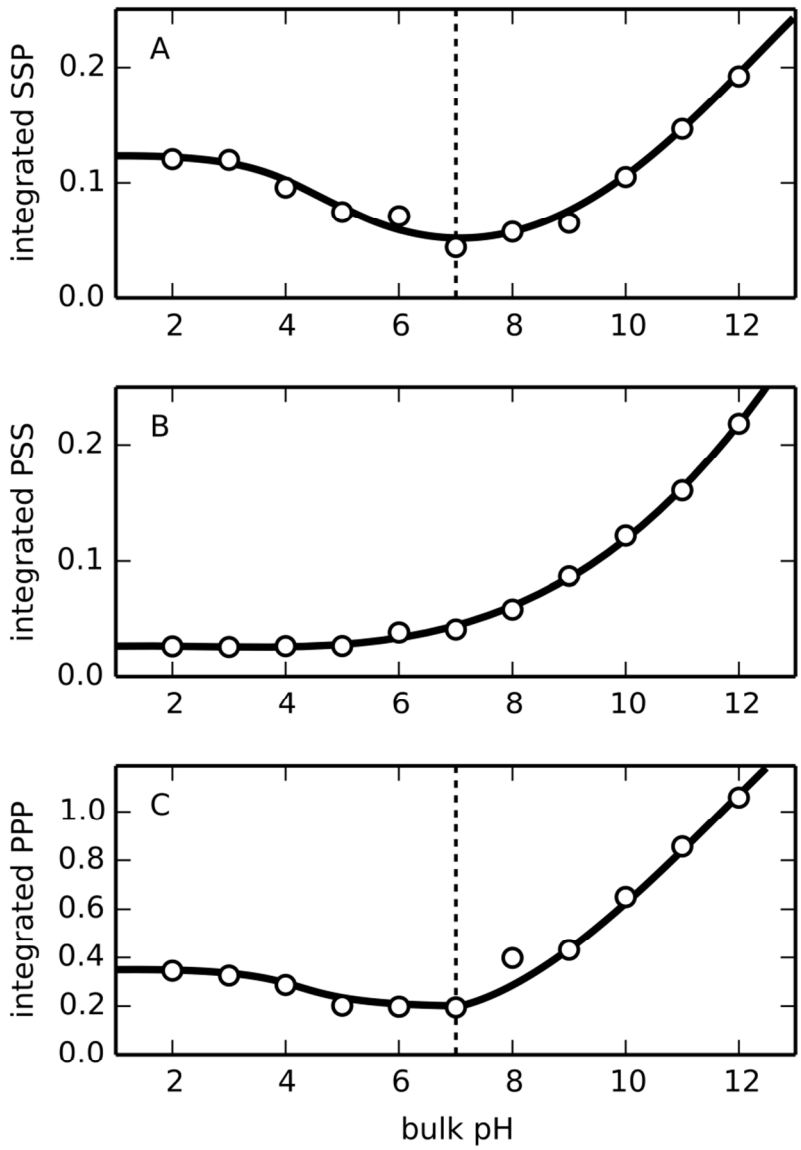


82x114mm (300 x 300 DPI)

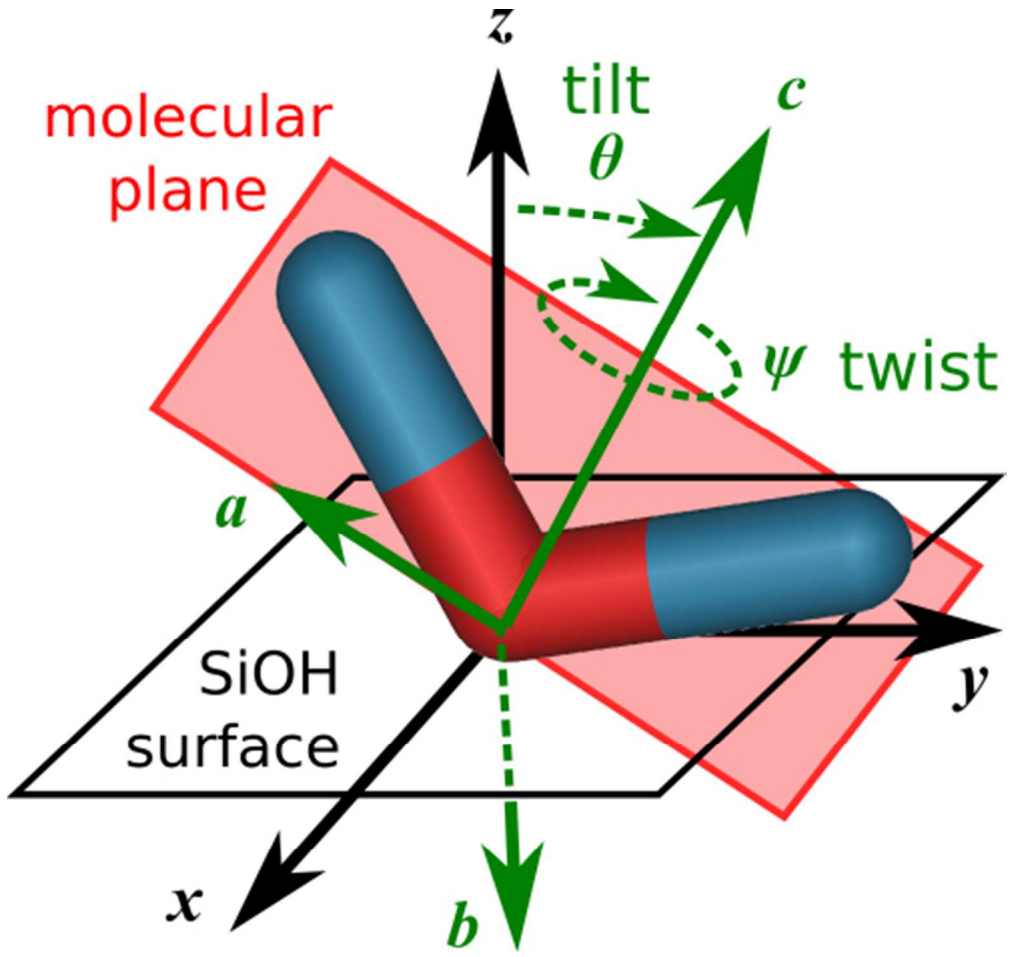


42x39mm (300 x 300 DPI)

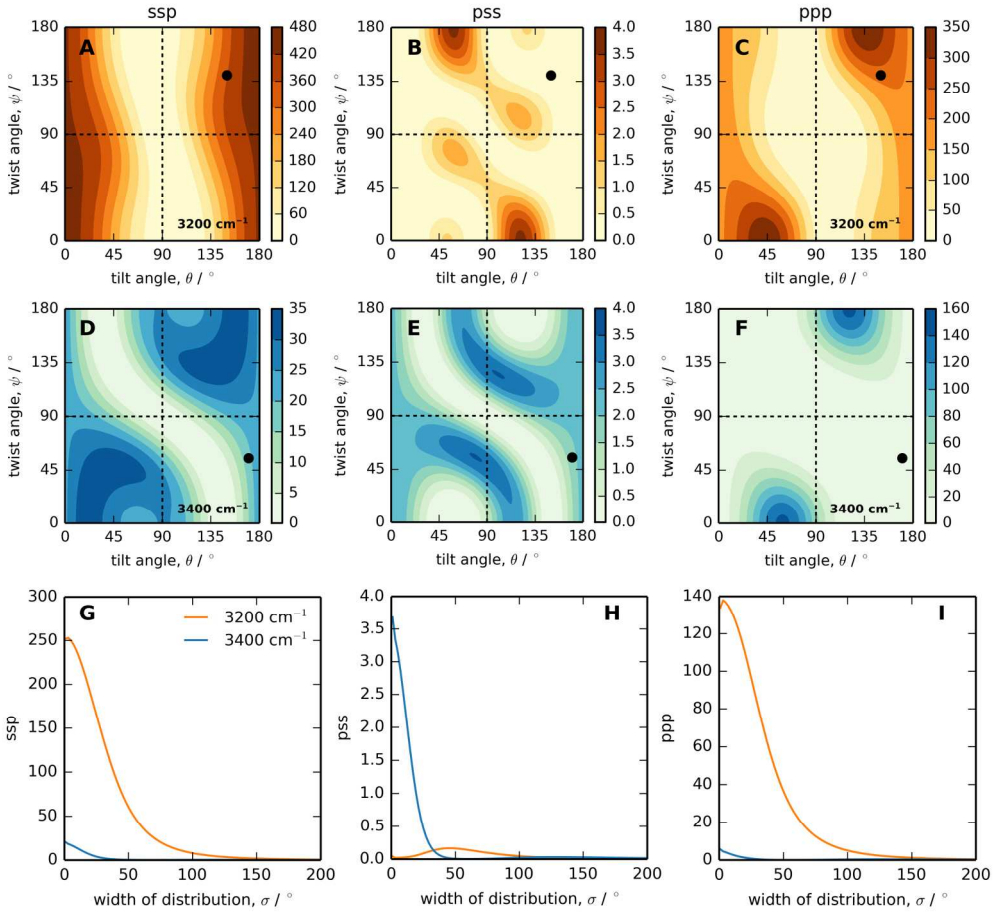


172x161mm (300 x 300 DPI)

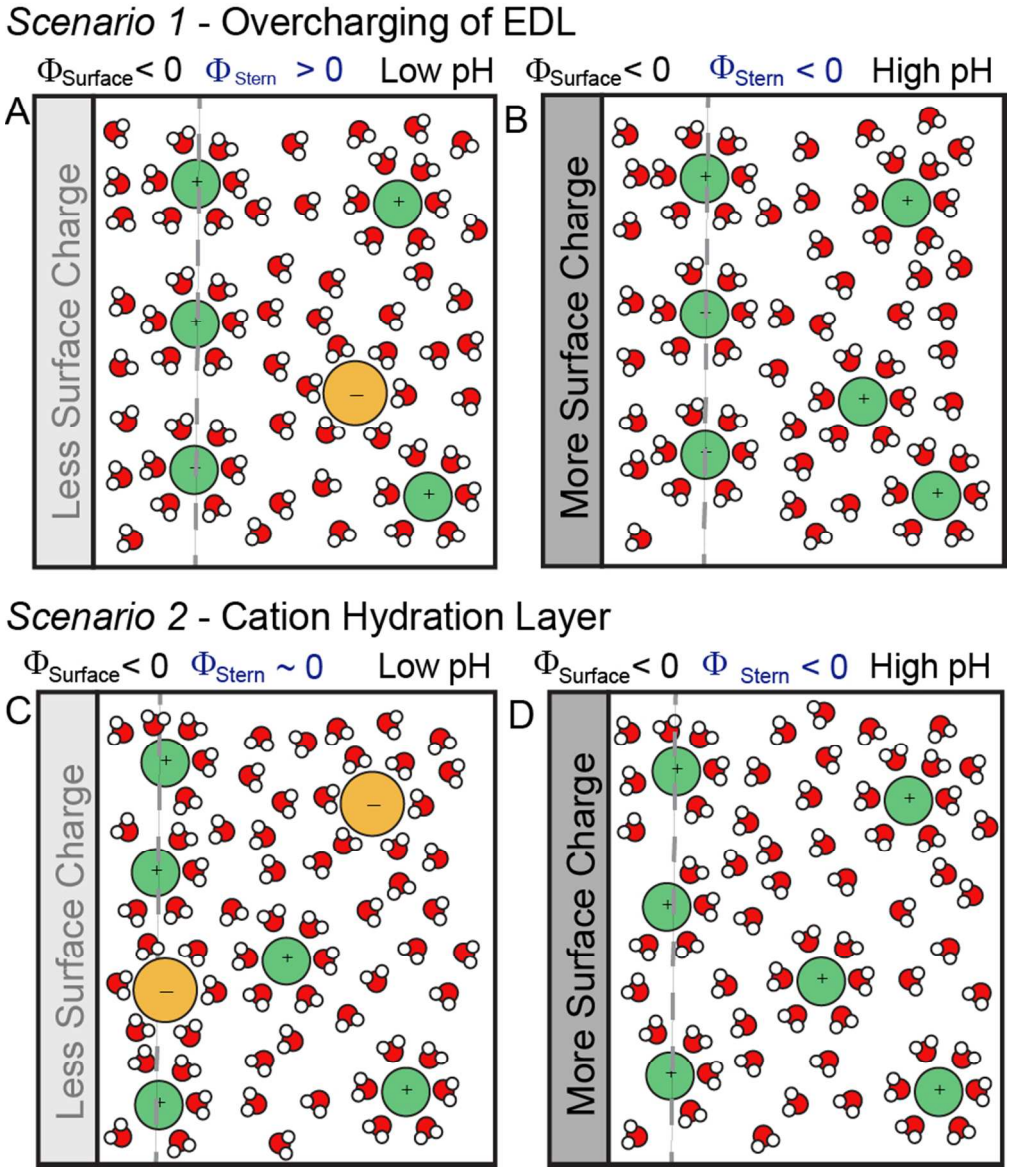


81x94mm (300 x 300 DPI)

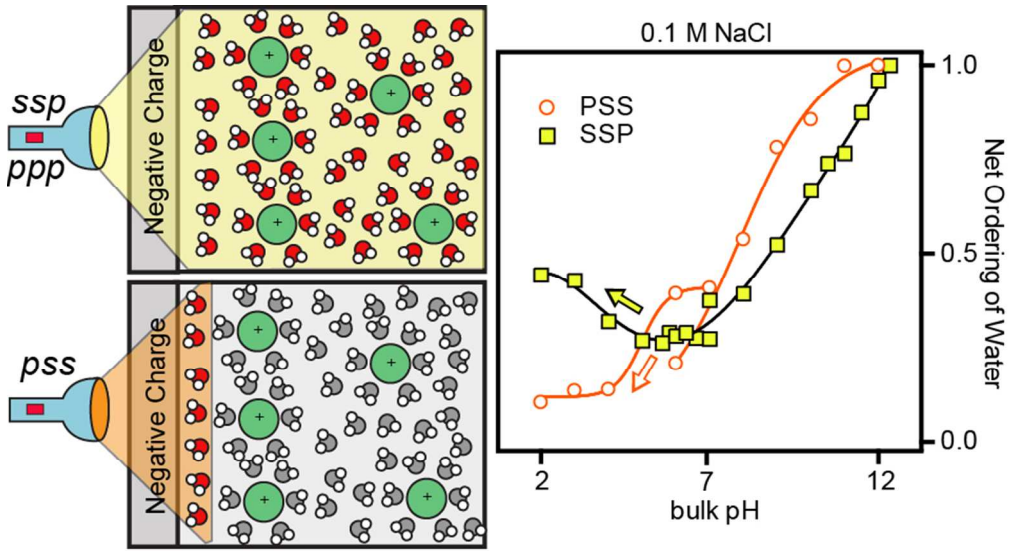


80x43mm (300 x 300 DPI)